



CERN-EP-2026-035
13 Feb 2026

Limits on the chiral magnetic effect from the event shape engineering and participant-spectator correlation techniques in Pb–Pb collisions at

$$\sqrt{s_{\text{NN}}} = 5.02 \text{ TeV}$$

ALICE Collaboration*

Abstract

The latest experimental studies related to the search for the Chiral Magnetic Effect (CME) in Pb–Pb collisions at $\sqrt{s_{\text{NN}}} = 5.02 \text{ TeV}$ recorded with the ALICE detector at the Large Hadron Collider (LHC) are presented. Charge-dependent two-particle correlations relative to the reaction plane are measured for charged particles in the pseudorapidity range $|\eta| < 0.8$ and the transverse-momentum range $0.2 < p_{\text{T}} < 5 \text{ GeV}/c$. Two approaches have been employed: in the first method, the contribution of the background to the measurement is varied using the event shape engineering (ESE), while the second relies on changing the contribution of the potential CME signal by measuring azimuthal correlations relative to the participant plane, where the background contributions are maximized, and spectator plane, where the CME signal contribution is maximized. Both methods yield results consistent with the absence of a CME signal within the measurement uncertainties. The result obtained from correlations relative to different symmetry planes, a technique applied for the first time at LHC energies, gives the possibility to test independently and confirm the upper limits from previous measurements, while the new limit from the ESE analysis offers improved constraint relative to previous attempts.

*See Appendix A for the list of collaboration members

1 Introduction

Ultra-relativistic heavy-ion collisions create the necessary conditions for the formation of a quark–gluon plasma (QGP), a state of matter in which quarks and gluons are deconfined and chiral symmetry is restored as a result of extreme temperatures and energy densities [1–3]. Theory expects that in a chirally restored medium such as the QGP [4], local parity violation could occur due to transitions of topologically non-trivial configurations of the gluonic field, coined as instantons and sphalerons, leading to a local imbalance of quark chirality [5–10]. In the initial-state of non-central collisions, spectator protons, i.e., those not participating directly in the interaction, generate extremely strong magnetic fields with magnitudes reaching up to 10^{15} T [11–13]. While the existence of these magnetic fields is theoretically well established, there is currently no direct experimental evidence for their effect on the motion of final-state particles since the field’s magnitude is expected to decay rapidly [14, 15]. The direction of the magnetic field is, on average, perpendicular to the reaction plane, which is defined by the impact parameter vector and the beam axis. In the presence of the initial-state magnetic field, the chirality imbalance could lead to the development of an electric current perpendicular to the reaction plane and parallel to the magnetic field. This phenomenon is known as the Chiral Magnetic Effect (CME) [9, 16] and is closely related to other anomalous phenomena such as the Chiral Separation Effect (CSE) [17], the Chiral Magnetic Wave (CMW) [18, 19], and the Chiral Vortical Effect (CVE) [20]. The CME manifests itself as a charge separation in the azimuthal distribution of produced particles relative to the reaction plane. The dominant component in the Fourier expansion of this distribution arises from anisotropic flow, a phenomenon originating from the initial-state asymmetry of the collision in coordinate space that is transformed into an anisotropy in momentum space via interactions between partons and at later stages between the produced particles. Anisotropic flow is usually characterized by the Fourier coefficients v_n in the expansion of the azimuthal distribution of produced particles [21, 22], with the first- (v_1) and second-order (v_2) coefficients corresponding to the directed and elliptic (the dominant harmonic) flow, respectively. In order to probe and quantify these local parity violation effects, one may introduce an additional sine component to this distribution, which takes the form

$$\frac{dN}{d\varphi_i} \sim 1 + 2 \sum_{n=1}^{\infty} [a_{n,i} \sin[n(\varphi_i - \Psi_{\text{RP}})] + v_{n,i} \cos[n(\varphi_i - \Psi_{\text{RP}})]], \quad (1)$$

where φ_i represents the azimuthal angle of particle i and Ψ_{RP} denotes the reaction plane angle. Due to fluctuations in the positions of nucleons within the colliding nuclei, the actual geometry of the overlapping region varies from one event to another [23–26]. This gives rise to additional symmetry planes, such as the participant plane (Ψ_{PP}), defined by the anisotropic distribution of participating nucleons and the spectator plane (Ψ_{SP}), determined by the deflected spectator nucleons. These planes are correlated to the reaction plane but fluctuate around it event-by-event. In Eq. 1, the first-order coefficient $a_{1,i}$ quantifies the magnitude of the local parity violation effect. Due to the spontaneous nature of the topological transitions, the effect averages to zero over many collision events [27]. This makes direct observation of $a_{1,i}$ challenging. Experimental techniques based on the study of charge-dependent azimuthal correlations are consequently developed to detect possible signatures of the CME [27]. These techniques are based on a charge-dependent azimuthal correlator

$$\gamma_{\alpha\beta} = \langle \cos(\varphi_{\alpha} + \varphi_{\beta} - 2\Psi_{\text{RP}}) \rangle = \langle \cos(\Delta\varphi_{\alpha}) \cos(\Delta\varphi_{\beta}) \rangle - \langle \sin(\Delta\varphi_{\alpha}) \sin(\Delta\varphi_{\beta}) \rangle, \quad (2)$$

where the angular brackets indicate an average over all events, and α and β denote the particle charge that allows to form particle pairs of opposite or same sign within the same event. The terms $\langle \cos(\Delta\varphi_{\alpha}) \cos(\Delta\varphi_{\beta}) \rangle$ and $\langle \sin(\Delta\varphi_{\alpha}) \sin(\Delta\varphi_{\beta}) \rangle$, with $\Delta\varphi_{\alpha,\beta} = \varphi_{\alpha,\beta} - \Psi_{\text{RP}}$, quantify the correlations with respect to the in- and out-of-plane directions, respectively. The CME sensitive observable is constructed by taking the difference of opposite-sign pairs γ_{+-} (OS) and same-sign pairs $(\gamma_{++} + \gamma_{--})/2$ (SS), and is denoted as $\Delta\gamma$. This reduces contributions from background associated with charge-independent sources.

The first results relying on this approach were published by the STAR Collaboration based on the analysis of Au–Au collisions at $\sqrt{s_{NN}} = 0.2$ TeV [28, 29]. Subsequent analyses [30–35] confirmed the observation of a result which initially seemed to be consistent with a charge separation relative to the reaction plane, in accordance to what is expected due to the CME. Quantitatively similar results were also reported at much higher energies at the Large Hadron Collider (LHC) [36–39]. It was later recognized that the measured $\Delta\gamma$ correlator contains substantial contribution from non-CME backgrounds [27, 40–46]. These backgrounds are primarily attributed to local charge conservation (LCC), i.e., the correlated emission of oppositely charged particles from a cluster, occurring within an anisotropically expanding medium, thereby mimicking the CME-like charge separation.

Lacking unambiguous evidence for the CME, the subsequent experimental studies focused on two approaches. In the first one, one tries to vary and quantify the background while keeping the contribution of the potential CME signal unaltered. Such an approach is embodied in the event shape engineering studies that allow to select events with different magnitude of elliptic flow within the same centrality [47]. This gives the possibility to quantify the dependence of $\Delta\gamma$ on one of the main background components, i.e., the elliptic flow. In the second approach, one modifies the signal contribution to $\Delta\gamma$ and looks for relative changes in the measurement. One example is experiments with isobar collisions at RHIC energies, which allowed to extract upper limits on the CME contribution to $\Delta\gamma$ [48, 49]. Another example are measurements of the charge-dependent correlations relative to different symmetry planes [50, 51]. This can be done by calculating the γ correlator relative to either Ψ_{PP} or Ψ_{SP} . The measurement relative to Ψ_{SP} will potentially have a bigger contribution from the CME signal since the charge separation takes place along the magnetic field predominantly created by spectator protons. At the same time, since the major background contribution comes from LCC convoluted with elliptic flow [27], which is a maximum in participant geometry, its contribution will be the largest when the azimuthal angles of the two particles are measured relative to Ψ_{PP} . Both approaches have been investigated so far and did not yield any significant evidence for the existence of the CME [35, 52, 53].

In this article, the results of the analysis of Pb–Pb collisions at $\sqrt{s_{NN}} = 5.02$ TeV recorded with ALICE at the LHC and based on the ESE technique and on correlations relative to Ψ_{PP} and Ψ_{SP} are presented. The article is organised as follows. Section 2 describes briefly the experimental layout and the data sample used, followed by a presentation of the two methods in Section 3. The systematic uncertainties of both measurements are discussed in Section 4. Section 5 presents the main results together with an overview of the new and previous ALICE findings. The final section contains the conclusion and outlook.

2 Experimental setup and data sample

The experimental setup of ALICE consists of a central barrel that contains several detectors and a set of forward systems [54]. Details about the various detector sub-systems and their performance can be found in Ref. [55].

Charged-particle tracks are reconstructed with the main tracking detectors, the Inner Tracking System (ITS) [56] and the Time Projection Chamber (TPC) [57], positioned in the central barrel inside a solenoid magnet which generates up to a 0.5 T field parallel to the beam direction. The ITS, during the first period of operation until 2019, consists of six layers of silicon detectors employing three different technologies: Silicon Pixel Detectors (SPD) for the two innermost layers, followed by two layers of Silicon Drift Detectors (SDD), and two outermost layers with double-sided Silicon Strip Detectors (SSD). The SPD layers are also employed for event selection and primary vertex reconstruction. The TPC, which surrounds the ITS, is used as the main tracking device as well as for particle identification via the measurement of the specific energy loss, dE/dx . In the forward region, two scintillator arrays (V0) [58] are used for triggering, event selection, the determination of the collision centrality [59] and participant plane. The V0 consists of two systems, the V0C and V0A, covering the pseudorapidity ranges $-3.7 < \eta < -1.7$ and

$2.8 < \eta < 5.1$, respectively. In addition, two tungsten-quartz neutron Zero Degree Calorimeters (ZDCs), installed more than 100 m from the interaction point on each side (ZDC-A and ZDC-C) and positioned at zero degree with respect to the LHC axis, are used for event selection and for the reconstruction of the spectator plane [60].

Approximately 235 million minimum-bias Pb–Pb events at $\sqrt{s_{NN}} = 5.02$ TeV recorded in 2018 are selected and analysed. The minimum-bias trigger is provided by requiring signals in both V0A and V0C scintillator arrays. An additional sample of central and semicentral collisions is selected online based on the V0 signal amplitudes, which enhanced the number of events in the 0–10% and 30–50% centrality ranges by about seven and three times relative to the minimum-bias sample, respectively. Beam-induced background events (i.e., beam–gas interactions) are removed offline utilizing the V0 and ZDC timing information [55]. Pileup of collisions from different bunch crossings in the TPC is rejected by comparing multiplicity estimates from the V0 detector to those of tracking detectors in the central barrel, profiting from the difference in readout times between the systems. The primary vertex position, determined from tracks reconstructed in the ITS and TPC, is required to be within 10 cm from the nominal interaction point along the beam direction. Events are classified in centrality intervals using the V0 detector; those in the 0–60% range of the total hadronic cross section are selected for the ESE analysis, while those in the 10–50% range are used for the participant/spectator-plane analysis. Residual systematic effects in the estimation of the spectator plane with the ZDC, related to beam optics configuration used during Pb–Pb data taking, were the reason for the difference in the centrality range used for the two approaches.

Primary charged particles reconstructed with the combination of the ITS and the TPC are required to be within the pseudorapidity range of $|\eta| < 0.8$. The transverse momentum is chosen to be within the range of $0.2 < p_T < 5.0$ GeV/ c for the ESE analysis and $0.2 < p_T < 3.0$ GeV/ c for the participant/spectator-plane analysis, respectively. These two p_T intervals have no influence on the final conclusion reported in this article. Results with the ESE method for $0.2 < p_T < 3.0$ GeV/ c did not show any significant difference relative to those reported in this article. Each charged-particle track is required to have a minimum number of 70 TPC space points out of a maximum of 159, a minimum number of crossed TPC pad rows of 70, an expected fraction of TPC space points to reconstruct a track of 0.8 and a χ^2 per TPC space point less than 2.5. In addition, tracks are selected if they had at least 2 hits in the six ITS layers, with a χ^2 per ITS hit less than 36. To ensure that secondary particles, either from a weak decay of primaries or from the interaction of particles with the detector material, are removed, a distance of closest approach (DCA) from the primary vertex smaller than 2 cm in the longitudinal direction is required. An additional DCA selection in the transverse plane was further applied based on a p_T -dependent maximum value of the form $0.0105 + 0.0350 p_T^{-1.1}$ cm. These selection criteria lead to an efficiency of about 80% for primary tracks with $p_T > 0.5$ GeV/ c , and a contamination by secondary charged particles of about 5% at $p_T = 1$ GeV/ c [61]. All results reported below are corrected for detector inefficiencies.

3 Analysis methods

For both analyses, the particles of interest are selected within the acceptance of the TPC. For the event shape engineering method, the q -vectors are calculated using hits within the acceptance of the V0 detectors. The same detectors are used in the second method for the reconstruction of the participant plane, while the ZDC detectors are used for the estimation of the spectator plane. The signal from both sets of detectors was corrected for detector anisotropies following the procedure described in previous studies [52, 60]. The choice of V0A or V0C used to construct the q -vectors and the participant plane follows the analysis configuration and is not expected to affect the extracted CME upper limits.

3.1 Event shape engineering

The selection on the shape of the event follows the prescription described in Ref. [47] and is based on the magnitude of the second-order normalized flow vector, q_2 [62], given by

$$q_2 = \frac{|\vec{Q}_2|}{\sqrt{M}}, \quad (3)$$

where \vec{Q}_2 is the second-order flow vector whose magnitude is $|\vec{Q}_2| = \sqrt{Q_{2,x}^2 + Q_{2,y}^2}$. The \vec{Q}_2 is determined from the azimuthal distribution of the energy deposition measured in the V0C detector with $Q_{2,x}$ and $Q_{2,y}$ being its x- and y-components calculated as

$$Q_{2,x} = \sum_i w_i \cos(2\varphi_i), \quad Q_{2,y} = \sum_i w_i \sin(2\varphi_i). \quad (4)$$

The sum runs over all channels i of the V0C detector ($i = 1 - 32$), φ_i is the azimuthal angle of channel i , w_i is the amplitude measured in channel i , and $M = \sum_i w_i$. The q_2 distribution is divided in percentiles from where ten event-shape classes are defined with the lowest (highest) q_2 value corresponding to the 0–10% (90–100%) range and are studied for each centrality interval. The results for each q_2 range correspond to the “biased” measurements, while the relevant results without any q_2 selection are referred to as “unbiased”.

The elliptic-flow coefficient is measured using the event-plane method [22] according to

$$v_2\{\text{EP}\} = \langle \langle \cos[2(\varphi_i - \Psi_2)] \rangle \rangle / \mathcal{R}_2, \quad (5)$$

where the brackets $\langle \langle \dots \rangle \rangle$ denote an average over all events and an average over all particles in all events. In addition, φ_i is the azimuthal angle of the particle of interest i measured in the TPC, and Ψ_2 , the second order event plane, estimates Ψ_{PP} . It is reconstructed from the azimuthal distribution of the energy deposition measured by the V0A detector as

$$\Psi_2^{\text{V0A}} = \text{atan2}[Q_{2,y}^{\text{V0A}}/Q_{2,x}^{\text{V0A}}]/2. \quad (6)$$

The event-plane resolution correction factor \mathcal{R}_2 in Eq. 5 is calculated from correlations between the event planes determined in the TPC and the two V0 detectors separately [22], and reaches a maximum value around 0.7–0.8 for the 10–40% centrality interval. Non-flow contributions to both v_2 and charge-dependent azimuthal correlations are suppressed by the large pseudorapidity separation between the TPC and the V0A ($|\Delta\eta| > 2.0$).

3.2 Charge-dependent correlations relative to different symmetry planes

This method, proposed in Refs. [50, 51], relies on the changes in the relative strength of the flow induced background and the potential CME signal when charge-dependent correlations are measured with respect to Ψ_{PP} or Ψ_{SP} planes. In particular, since the background depends on the elliptic-flow magnitude which, when calculated from correlations between two particles, is maximum in the participant plane, its contribution to $\Delta\gamma$ will be enhanced or reduced when the charge-dependent correlations are measured relative to Ψ_{PP} or Ψ_{SP} , respectively. Inversely, since the CME signal is proportional to the value of the magnetic field which is mainly determined by the spectator protons, measurements performed relative to Ψ_{SP} will have larger contribution from it than when the same measurements are performed with respect to Ψ_{PP} . One can then form the double ratio $(\Delta\gamma/v_2)_{\text{SP}}/(\Delta\gamma/v_2)_{\text{PP}}$ which is expected to be larger than unity in the case of non-zero CME. In that case the double ratio can be used to estimate the relative contribution of the CME to $\Delta\gamma$, expressed as the fraction f_{CME} . Assuming that both the spectator plane and the plane perpendicular to the magnetic field coincide, the f_{CME} can be extracted according to

$$\frac{(\Delta\gamma/v_2)_{\text{SP}}}{(\Delta\gamma/v_2)_{\text{PP}}} = 1 + f_{\text{CME}} \left(\frac{\langle v_{2,\text{PP}}^2 \rangle}{v_{2,\text{SP}}^2} - 1 \right). \quad (7)$$

In Ref. [51], it was noticed that the ratio $\Delta\gamma/v_2$ can be measured directly as

$$(\Delta\gamma/v_2)_{\text{PP,SP}} = \frac{\Delta\langle\cos(\varphi_\alpha + \varphi_\beta - 2\Psi_{\text{PP,SP}})\rangle}{\langle\cos(2\varphi_a - 2\Psi_{\text{PP,SP}})\rangle}, \quad (8)$$

which does not require the knowledge of the reaction-plane resolution, and thus could be measured more precisely. In our measurements, the spectator plane is calculated from the combined signal of the two ZDC detectors on the A- and C-sides using equation analogous to Eq. 4 for a first harmonic [63] to calculate the corresponding Q-vectors $\vec{Q}^{\text{ZDC-A}}$ and $\vec{Q}^{\text{ZDC-C}}$, and Ψ_{PP} is estimated using the V0C detector. Similarly to the previous method, the v_2 is measured using the event-plane method [22]. The large pseudorapidity difference between the TPC, where the particles of interest for both the calculation of γ and v_2 are reconstructed, and the V0C detector in one case or the ZDC in the other case, ensures a significant reduction of non-flow contributions to the measurement.

4 Systematic uncertainties

The systematic uncertainties for both methods are evaluated by commonly varying the selection criteria at both the event and track levels for both analyses. All common sources listed below are investigated for the biased and unbiased results for same- and opposite-sign charge combinations in γ , as well as for v_2 for the ESE method. Similarly, for the double ratio in Eq. 8, the results of correlations relative to different symmetry planes for each centrality interval are studied separately for the various charge combinations for γ as well as for v_2 . This procedure allowed to take into account any correlations between the different components that form the more complex observables (e.g. Eq. 7) reported in this article. Only statistically significant differences of more than 2σ between the values of the nominal data points and the results from the variations are assigned as systematic uncertainties according to Ref. [64]. The contributions from the various independent sources are added in quadrature to obtain the final systematic uncertainties on each of the measurements. These are represented with a box around each data point, while the statistical uncertainties are denoted by vertical bars in all figures of this article.

Systematic effects originating from the variation of the acceptance of the detector are investigated by varying the range of the position of the reconstructed primary vertex on the z-axis from its default value of $|V_z| < 10$ cm down to $|V_z| < 5$ cm. Potential biases coming from the centrality determination are studied by replacing the V0 detector amplitude by the total number of hits detected in two SPD layers. Systematic effects originating from the magnetic-field polarity are studied by analyzing events recorded under different magnetic field polarities independently. In addition, the influence of pileup events to both measurements is estimated by either completely removing the pileup requirements or by imposing stricter selections. Effects introduced by the different track selection criteria are checked for both analyses by varying the minimum number of TPC space points (i.e., from 70 to 90), the minimum number of crossed TPC pad rows and the expected fraction of TPC space points to reconstruct a track (i.e., from 70 to 120 and from 0.8 to 0.9, respectively), and by imposing tighter DCA requirements that reduce the contribution from secondary particles to the track sample. Biases from the detector combination used to perform track reconstruction are tested by employing an alternative method, referred to as global tracking. This mode combines the TPC and ITS detector signals and incorporates stricter selection criteria, including additional hit requirements in the SPD or SDD detectors. In addition, for both methods, the results for same-sign correlations obtained using the combination of only positive or only negative particles are compared and found to be compatible. Finally, potential biases introduced by the inaccurate estimation of the reconstruction efficiency are studied by either not applying any efficiency corrections or by estimating these corrections after excluding the contribution from strange and multi-strange particles. Among these common sources, the dominant contributions for the ESE method are associated with the centrality determination and the alternative track reconstruction configuration (global tracking), whereas for the (PP/SP) method the dominant contribution is discussed below.

In addition to the previous common contributions, the (PP/SP) method includes an extra source related to noticeable un-physical off-diagonal correlations $\langle XY \rangle$ ($\langle Q_x^{\text{ZDC-C}} Q_y^{\text{ZDC-A}} \rangle$) and $\langle YX \rangle$ ($\langle Q_y^{\text{ZDC-C}} Q_x^{\text{ZDC-A}} \rangle$) components even after the ZDC signal calibration. These residual non-zero values for $\langle XY \rangle$ and $\langle YX \rangle$ are due to detector and beam-related artefacts. They could arise from a small rotation or shear of the spectator-neutron spot at the ZDC location due to the specific heavy-ion beam optics during the LHC operations (e.g. beam divergence and crossing angle), combined with remaining misalignment of the ZDCs with respect to the interaction region and their response non-uniformities. These effects can lead to an effective mixing of the X and Y components that is not removed by the signal correction procedure [65]. This residual correlation affects the values of $\cos(n\Psi_{\text{SP}}^{\text{ZDC-C,ZDC-A}})$ and $\sin(n\Psi_{\text{SP}}^{\text{ZDC-C,ZDC-A}})$. To evaluate the potential impact on $\Delta\gamma_{\text{SP}}$ and $v_{2,\text{SP}}$, the approach used in Ref. [65] is adopted, where the values of these observables are scaled by a factor (F_{ZDC}) to estimate any residual effects

$$F_{\text{ZDC}} = \sqrt{\frac{\langle Q_x^{\text{ZDC-C}} Q_y^{\text{ZDC-A}} \rangle \langle Q_y^{\text{ZDC-C}} Q_x^{\text{ZDC-A}} \rangle}{\langle Q_x^{\text{ZDC-C}} Q_x^{\text{ZDC-A}} \rangle \langle Q_y^{\text{ZDC-C}} Q_y^{\text{ZDC-A}} \rangle}}. \quad (9)$$

For the (PP/SP) method, the event-plane resolution for both Ψ_{SP} and Ψ_{PP} cancel out in the ratio ($\Delta\gamma/v_2$) [51]. However, extracting the CME fraction from Eq. 7 requires accounting for the event-plane resolutions of both Ψ_{PP} and Ψ_{SP} in the ratio $\langle v_{2,\text{PP}}^2 \rangle / v_{2,\text{SP}}^2$. Since the resolution of the spectator plane could not be directly determined using the ALICE ZDC detector for the Pb–Pb events at $\sqrt{s_{\text{NN}}} = 5.02$ TeV recorded in 2018, we assume that the ratio $v_{2,\text{SP}}/v_{2,\text{PP}}$ is independent of the collision energy

$$\frac{v_{2,\text{SP}}(5.02 \text{ TeV})}{v_{2,\text{PP}}(5.02 \text{ TeV})} = \frac{v_{2,\text{SP}}(2.76 \text{ TeV})}{v_{2,\text{PP}}(2.76 \text{ TeV})}, \quad (10)$$

where the spectator-plane resolution for the Pb–Pb events at $\sqrt{s_{\text{NN}}} = 2.76$ TeV recorded in 2010 was successfully determined [65]. The ratio primarily reflects the strength of flow fluctuations, i.e., the decorrelation between the reaction plane and the participant plane due to initial-geometry fluctuations. These fluctuations are determined by the transverse nucleon distribution and are not expected to vary significantly with LHC energies [66, 67]. In addition, none of the common sources of systematic uncertainty results in a statistically significant deviation greater than 2σ in the double ratio. This shows that the double ratio is particularly effective in canceling out systematic uncertainties that are unrelated to the spectator-plane reconstruction. The only contribution to the systematic uncertainty in the double ratio originates from the biases in the estimation of the spectator plane, whose magnitude is comparable to the statistical uncertainty.

5 Results

5.1 Event shape engineering

The top panel of Fig. 1 presents the centrality dependence of v_2 for inclusive charged particles measured in $0.2 < p_{\text{T}} < 5.0$ GeV/ c and $|\eta| < 0.8$ for shape-selected and unbiased samples. The event shape-selected results differ from the average by up to 30%. These differences vary strongly with centrality as the sensitivity of the event selection depends on multiplicity and the magnitude of v_2 [68]. Furthermore, v_2 scales approximately linearly with eccentricity [69] verifying that with the ESE method events with different eccentricity (i.e., initial spatial anisotropy) and, therefore, with different background contribution are experimentally selected in a given centrality interval.

The bottom panel of Fig. 1 shows the centrality dependence of $\gamma_{\alpha\beta}$ for same- and opposite-sign pairs. Since the results for pairs of particles with only positive charges are consistent with those for negative charges, they are averaged and denoted as same-sign pairs in all figures and for both methods. Similarly to what is reported in previous measurements [52], a clear dependence on the charge-sign combination

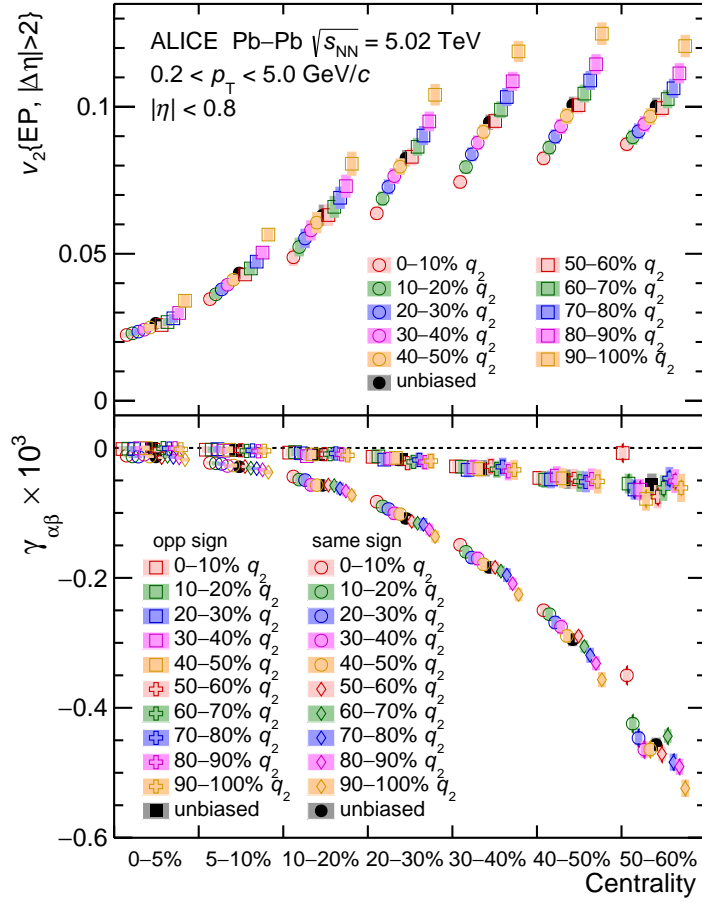


Figure 1: Centrality dependence of inclusive charged particle v_2 (top) and of $\gamma_{\alpha\beta}$ for pairs of particles with same and opposite sign (bottom) for shape-selected and unbiased events. The q_2 determined in the V0C is used for event selection. Statistical and systematic uncertainties are represented by vertical lines and shaded boxes, respectively.

is exhibited by $\gamma_{\alpha\beta}$ with the opposite-sign pair correlations being weaker than the same-sign pair ones for both unbiased and shape-selected events. The magnitude of the same-sign pair correlations decreases from central to peripheral collisions and depends on the event-shape selection (i.e., v_2) in a given centrality interval. The magnitude of opposite-sign pair correlations is close to zero with a weak (if any) dependence on v_2 within a given centrality interval.

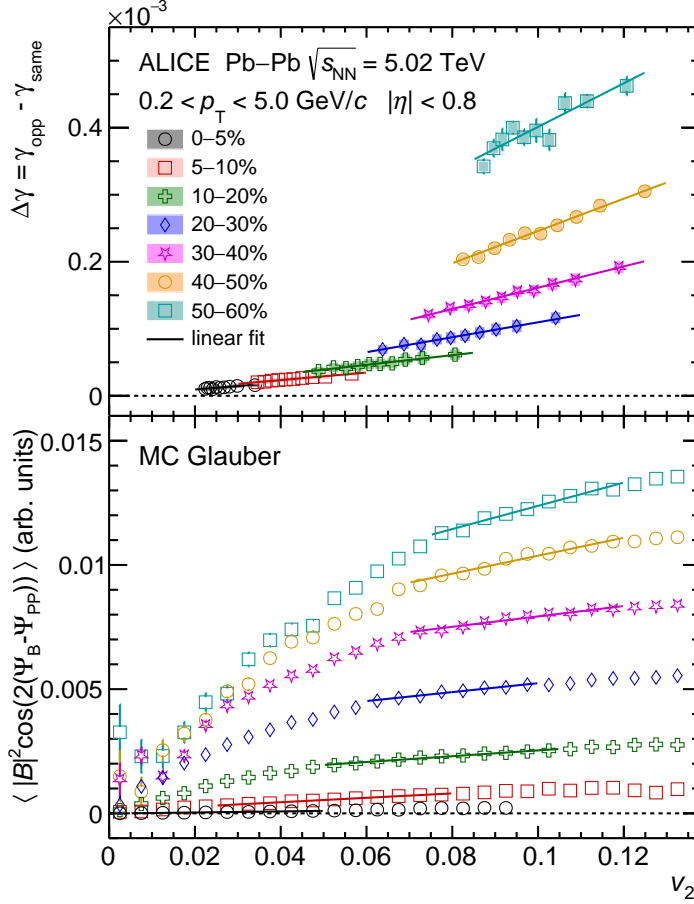


Figure 2: The dependence of $\Delta\gamma_{\alpha\beta}$ (top) and of the expected CME signal from a MC Glauber simulation [70] (bottom) on v_2 together with linear fits (solid lines) for various centrality intervals. For the model, no event shape selection is performed and the range of the fit is based on the v_2 variation observed in data within each centrality class. Statistical and systematic uncertainties are represented by vertical lines and shaded boxes, respectively.

In a background-dominated scenario, the charge-dependent effects, reflected in the charge-dependent differences $\Delta\gamma$, would be proportional to v_2 for all centrality intervals. The upper panel of Fig. 2 presents the dependence of $\Delta\gamma$ on the main background gauge, i.e., v_2 , for various ESE selections within each centrality interval. It is seen that $\Delta\gamma$ is positive and exhibits a clear linear dependence on v_2 , also illustrated by the linear functions fitted on each set of data points. In addition, $\Delta\gamma$ has a clear centrality dependence, with the values progressively increasing when moving from central to peripheral events. This is expected considering dilution effects [71] introduced by the higher multiplicity in central compared with peripheral events.

The bottom panel of Fig. 2 shows the v_2 dependence of the expected CME signal from a MC Glauber simulation [70] for various centrality intervals. The CME signal contribution to $\Delta\gamma$ is assumed to be proportional to $\langle |B|^2 \cos[2(\Psi_B - \Psi_{PP})] \rangle$, where Ψ_B and $|B|$ are the direction and magnitude of the magnetic field, respectively. The magnetic field is evaluated at the geometrical center of the overlap region from

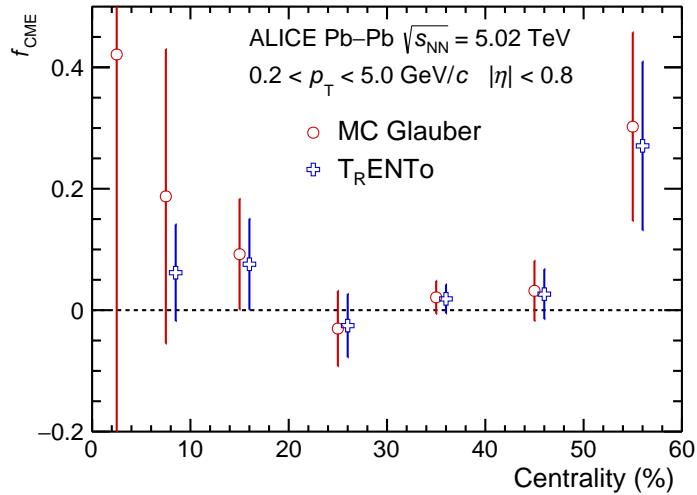


Figure 3: Centrality dependence of the CME fraction extracted from the slope parameter of fits to data and MC Glauber [70] and T_RENTo [73] models (see text for details). The T_RENTo points are slightly shifted along the horizontal axis for better visibility. Only statistical uncertainties are shown.

the number of spectator protons with the proper time $\tau = 0.1$ fm/c according to the recipe discussed in Ref. [9]. The elliptic flow calculated from the model reproduces fairly well the measured integrated v_2 [72] under the assumption that it scales linearly with eccentricity calculated from the distribution of participant nucleons. Centrality is determined as in Ref. [52] from the multiplicity of charged particles generated in the V0 acceptance using the parameters reported in Ref. [59]. A strong dependence on v_2 is found for all centrality intervals, which is also reproduced by a MC simulation using T_RENTo initial conditions [73].

Following the approach described in Ref. [52], the v_2 dependence of $\Delta\gamma$ and that of the expected CME signal are fitted with linear functions in the range that matches the one measured in collision data for each centrality interval presented in the upper panel of Fig. 1. The slopes from data and MC models are used to calculate the CME fraction to the charge dependence of $\gamma_{\alpha\beta}$, denoted as f_{CME} . Figure 3 shows the centrality dependence of f_{CME} for the MC Glauber and T_RENTo models. The CME fraction cannot be precisely determined for the 0–5% centrality interval where models have difficulties in reproducing the experimental data [74]. The values of f_{CME} are compatible with zero for most of the investigated centrality classes. The reduced sensitivity of the event selection (e.g. with the ESE) contributes to the large values obtained in the 50–60% centrality interval. Neglecting any centrality dependence for the 5–60% centrality interval, the CME fraction obtained by fitting the data points with a constant function is $f_{\text{CME}} = 0.028 \pm 0.021$ and $f_{\text{CME}} = 0.025 \pm 0.018$ for MC Glauber and T_RENTo initial conditions, respectively. These values correspond to upper limits for the CME fraction in $\Delta\gamma$ of 7% and 6% at 95% confidence level for the 5–60% centrality interval.

5.2 Charge-dependent correlations relative to different symmetry planes (PP/SP)

Figure 4 presents the centrality dependence of $\gamma_{\alpha\beta}(\Psi_{\text{PP}})/v_2(\Psi_{\text{PP}})$ and $\gamma_{\alpha\beta}(\Psi_{\text{SP}})/v_2(\Psi_{\text{SP}})$, where pairs of particles in $\gamma_{\alpha\beta}$ are either of the same or opposite charge. A significant charge dependence that develops as a function of centrality is observed in both category of results. Moreover, it is seen that the two results do not exhibit any significant differences for a given charge combination.

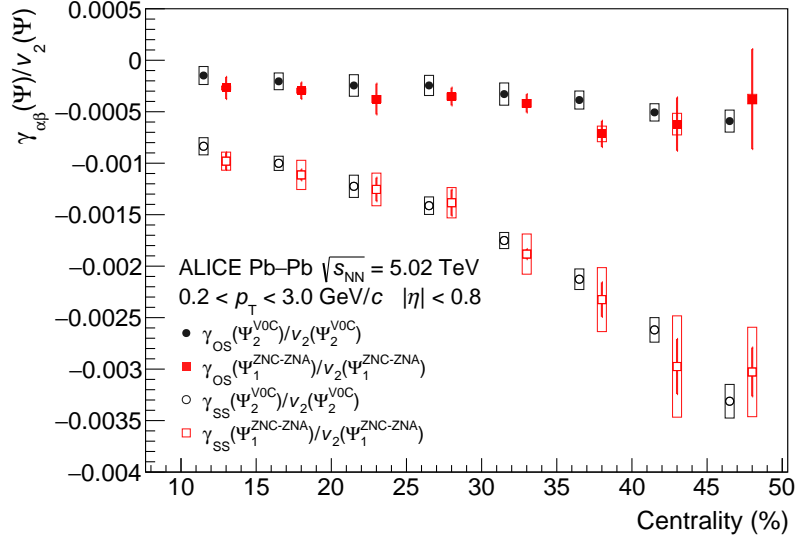


Figure 4: Centrality dependence of $\gamma_{\alpha\beta}(\Psi_{PP})/v_2(\Psi_{PP})$ (black) and $\gamma_{\alpha\beta}(\Psi_{SP})/v_2(\Psi_{SP})$ (red), where pairs of particles in $\gamma_{\alpha\beta}$ are either of the same charge or the opposite charge in Pb–Pb collisions at $\sqrt{s_{NN}} = 5.02$ TeV. Filled markers correspond to OS correlations, open markers to SS correlations, with vertical bars representing statistical uncertainties and boxes representing systematic uncertainties.

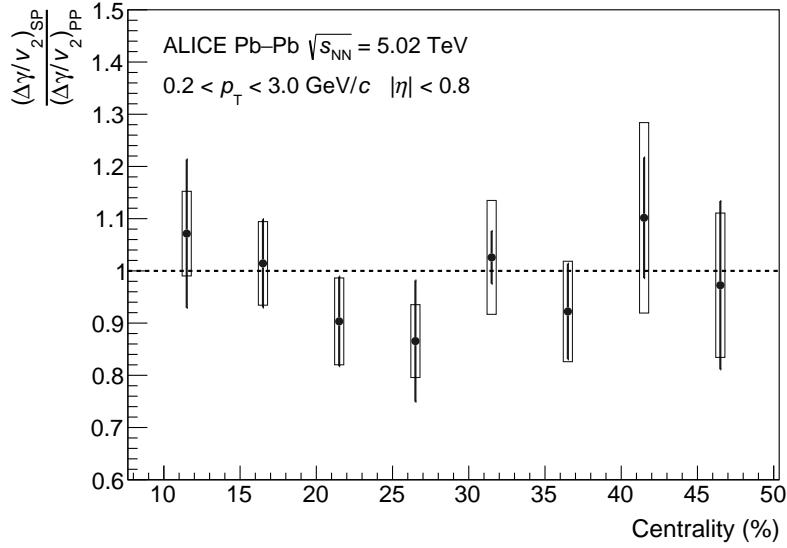


Figure 5: The double ratio of $\Delta\gamma/v_2$ in Eq. 7 calculated with the spectator and participant planes as a function of centrality in Pb–Pb collisions at $\sqrt{s_{NN}} = 5.02$ TeV. The vertical bars and boxes represent statistical and systematic uncertainties, respectively.

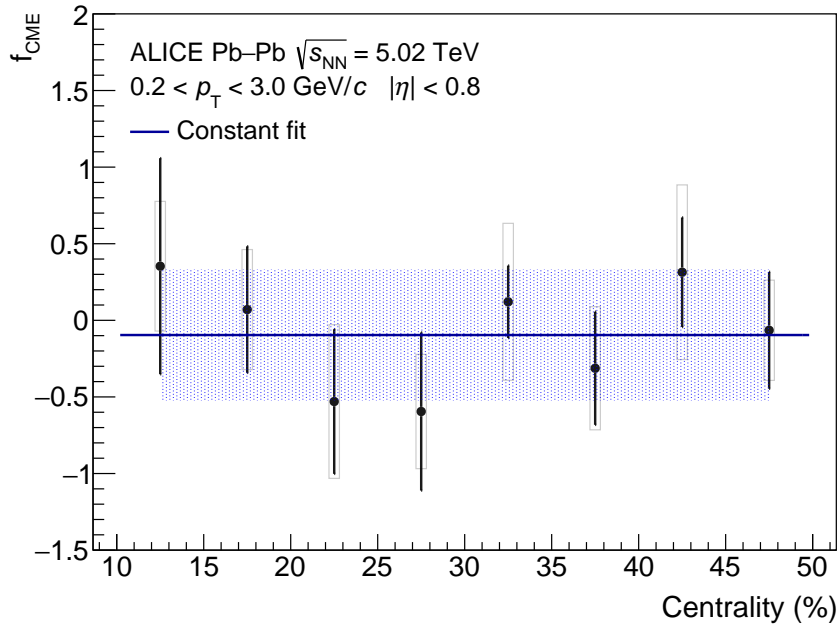


Figure 6: The centrality dependence of f_{CME} extracted from correlations measured relative to the spectator and participants planes according to Eq. 7 in Pb–Pb collisions at $\sqrt{s_{\text{NN}}} = 5.02$ TeV. Statistical uncertainties are shown as vertical bars, and systematic uncertainties are shown as boxes. A constant fit is shown along with a 95% confidence level band.

To quantify the difference, the result of the double ratios in Eq. 8 is shown in Fig. 5. The double ratios in the centrality range of 10–30% are measured with the minimum-bias trigger, while those in the 30–50% centrality range are measured with the dedicated trigger that enhances events in this centrality interval. The double ratio is compatible with unity within the statistical and systematic uncertainties throughout the centrality range 10–50%.

Figure 6 shows the extracted f_{CME} as a function of centrality using the procedure described in Sec. 3.2 and Eq. 7. A constant line fit to f_{CME} considering the total uncertainty that includes both statistical and systematic uncertainties in the centrality range of 10–50% yields a value of -0.096 ± 0.214 . This translates to an upper limit for the CME fraction in $\Delta\gamma$ of 33% at a 95% confidence level.

5.3 ALICE summary of upper limits for the CME fraction in $\Delta\gamma$

Figure 7 presents a summary of the upper limits reported by ALICE for the CME signal contribution to $\Delta\gamma$. These values are obtained from different analyses performed at various LHC energies and colliding systems integrated over centralities in Run 1 and Run 2. These include the data points from previous ESE studies [52] incorporating results from three initial-state models, higher harmonics at two different LHC energies [75], as well as from the comparison of correlations in Xe–Xe and Pb–Pb collisions using a two-component model [44]. The initial ESE results provided the first upper limits at the LHC of around 26–33% at 95% confidence level [52], while the ones from the higher harmonic study that rely on specific assumptions discussed in detail in Ref. [75] reported similar limits of around 15–18% at 95% confidence level. Finally, in Ref. [44] ALICE reported an upper limit of around 2% and 25% at 95% confidence level for the 0–70% centrality interval in Xe–Xe and Pb–Pb collisions, respectively. The main reason for the low upper limit reported in the Xe–Xe system is related to the significantly lower magnetic field value this system creates relative to the Pb–Pb one. The measurements reported in this article add significant information to the existing set of results.

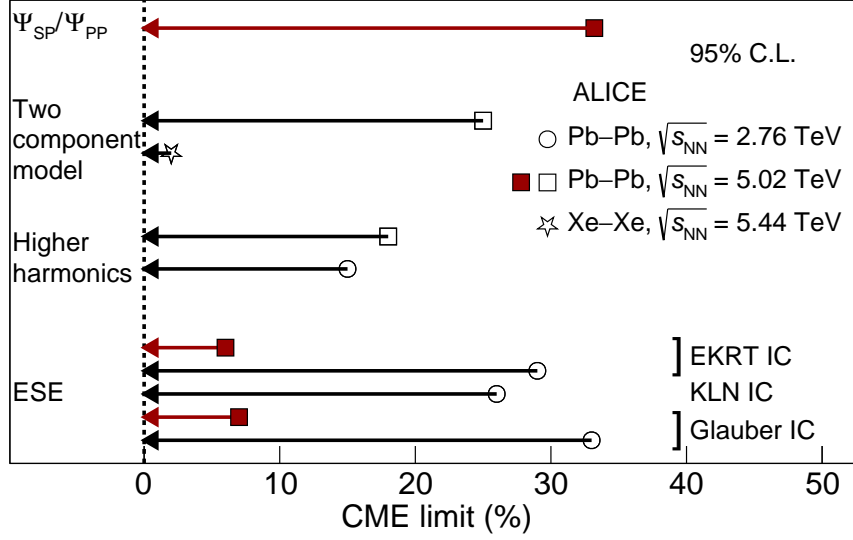


Figure 7: Summary of the results for the CME limit at 95% confidence level (C.L.) obtained from different analyses for different colliding systems at various energies at the LHC integrated over centralities from ALICE. The previous measurements are taken from Refs. [44, 52, 75] and are represented with the open markers.

6 Summary

In this article, the results from the analysis of Pb–Pb collisions at $\sqrt{s_{NN}} = 5.02$ TeV collected with the ALICE detector using two independent methods are reported. The charge-dependent correlations are studied using the correlator $\gamma_{\alpha\beta}$ with the ESE technique and by measuring correlations relative to the participant and spectator planes. These two methods have distinctively different sensitivities to the background originating from local charge conservation effects embedded in an anisotropically expanding system and the potential CME signal. Both methods reported significant charge-dependent effects, which, however, are compatible with a dominant background contribution. In both cases upper limits for the CME fraction in $\Delta\gamma$ of 7% and 6% at 95% confidence level for the 5–60% centrality interval and 33% at a 95% confidence level for the 10–50% centrality interval, respectively, are reported. These results, while having different uncertainties due to experimental techniques, are equally important for the CME search and complement the limits obtained from previous relevant measurements at LHC energies. With the significantly larger data sample from Run 3 and Run 4, analyses based on ESE and correlations relative to different symmetry planes will achieve higher precision. In addition, new measurements involving identified particle species [76] and the use of the ZDC as a sensitive probe of the magnetic field [77] will provide complementary avenues to further advance in the CME search.

Acknowledgements

The ALICE Collaboration would like to thank all its engineers and technicians for their invaluable contributions to the construction of the experiment and the CERN accelerator teams for the outstanding performance of the LHC complex. The ALICE Collaboration gratefully acknowledges the resources and support provided by all Grid centres and the Worldwide LHC Computing Grid (WLCG) collaboration. The ALICE Collaboration acknowledges the following funding agencies for their support in building and running the ALICE detector: A. I. Alikhanyan National Science Laboratory (Yerevan Physics Institute) Foundation (ANSL), State Committee of Science and World Federation of Scientists (WFS), Armenia; Austrian Academy of Sciences, Austrian Science Fund (FWF): [M 2467-N36] and National-

stiftung für Forschung, Technologie und Entwicklung, Austria; Ministry of Communications and High Technologies, National Nuclear Research Center, Azerbaijan; Rede Nacional de Física de Altas Energias (Renafae), Financiadora de Estudos e Projetos (Finep), Fundação de Amparo à Pesquisa do Estado de São Paulo (FAPESP) and The Sao Paulo Research Foundation (FAPESP), Brazil; Bulgarian Ministry of Education and Science, within the National Roadmap for Research Infrastructures 2020-2027 (object CERN), Bulgaria; Ministry of Education of China (MOEC), Ministry of Science & Technology of China (MSTC) and National Natural Science Foundation of China (NSFC), China; Ministry of Science and Education and Croatian Science Foundation, Croatia; Centro de Aplicaciones Tecnológicas y Desarrollo Nuclear (CEADEN), Cubaenergía, Cuba; Ministry of Education, Youth and Sports of the Czech Republic, Czech Republic; The Danish Council for Independent Research | Natural Sciences, the VILLUM FONDEN and Danish National Research Foundation (DNRF), Denmark; Helsinki Institute of Physics (HIP), Finland; Commissariat à l’Energie Atomique (CEA) and Institut National de Physique Nucléaire et de Physique des Particules (IN2P3) and Centre National de la Recherche Scientifique (CNRS), France; Bundesministerium für Forschung, Technologie und Raumfahrt (BMFTR) and GSI Helmholtzzentrum für Schwerionenforschung GmbH, Germany; National Research, Development and Innovation Office, Hungary; Department of Atomic Energy Government of India (DAE), Department of Science and Technology, Government of India (DST), University Grants Commission, Government of India (UGC) and Council of Scientific and Industrial Research (CSIR), India; National Research and Innovation Agency - BRIN, Indonesia; Istituto Nazionale di Fisica Nucleare (INFN), Italy; Japanese Ministry of Education, Culture, Sports, Science and Technology (MEXT) and Japan Society for the Promotion of Science (JSPS) KAKENHI, Japan; Consejo Nacional de Ciencia (CONACYT) y Tecnología, through Fondo de Cooperación Internacional en Ciencia y Tecnología (FONCICYT) and Dirección General de Asuntos del Personal Académico (DGAPA), Mexico; Nederlandse Organisatie voor Wetenschappelijk Onderzoek (NWO), Netherlands; The Research Council of Norway, Norway; Pontificia Universidad Católica del Perú, Peru; Ministry of Science and Higher Education, National Science Centre and WUT ID-UB, Poland; Korea Institute of Science and Technology Information and National Research Foundation of Korea (NRF), Republic of Korea; Ministry of Education and Scientific Research, Institute of Atomic Physics, Ministry of Research and Innovation and Institute of Atomic Physics and Universitatea Nationala de Stiinta si Tehnologie Politehnica Bucuresti, Romania; Ministerstvo školstva, vyzkumu, vyvoja a mladeze SR, Slovakia; National Research Foundation of South Africa, South Africa; Swedish Research Council (VR) and Knut & Alice Wallenberg Foundation (KAW), Sweden; European Organization for Nuclear Research, Switzerland; Suranaree University of Technology (SUT), National Science and Technology Development Agency (NSTDA) and National Science, Research and Innovation Fund (NSRF via PMU-B B05F650021), Thailand; Turkish Energy, Nuclear and Mineral Research Agency (TENMAK), Turkey; National Academy of Sciences of Ukraine, Ukraine; Science and Technology Facilities Council (STFC), United Kingdom; National Science Foundation of the United States of America (NSF) and United States Department of Energy, Office of Nuclear Physics (DOE NP), United States of America. In addition, individual groups or members have received support from: FORTE project, reg. no. CZ.02.01.01/00/22_008/0004632, Czech Republic, co-funded by the European Union, Czech Republic; European Research Council (grant no. 950692), European Union; Deutsche Forschungs Gemeinschaft (DFG, German Research Foundation) “Neutrinos and Dark Matter in Astro- and Particle Physics” (grant no. SFB 1258), Germany; FAIR - Future Artificial Intelligence Research, funded by the NextGenerationEU program (Italy).

References

- [1] E. V. Shuryak, “Quark-Gluon Plasma and Hadronic Production of Leptons, Photons and Psions”, *Phys. Lett. B* **78** (1978) 150.
- [2] F. Karsch and E. Laermann, “Thermodynamics and in medium hadron properties from lattice QCD”, *World Scientific* (2004) 1–59, arXiv:hep-lat/0305025.

- [3] A. Bazavov *et al.*, “Equation of state and QCD transition at finite temperature”, *Phys. Rev. D* **80** (2009) 014504, arXiv:0903.4379 [hep-lat].
- [4] **HotQCD** Collaboration, A. Bazavov *et al.*, “Chiral crossover in QCD at zero and non-zero chemical potentials”, *Phys. Lett. B* **795** (2019) 15–21, arXiv:1812.08235 [hep-lat].
- [5] P. Morley and I. Schmidt, “Strong P, CP, T Violations in Heavy Ion Collisions”, *Z. Phys. C* **26** (1985) 627.
- [6] D. Kharzeev, R. Pisarski, and M. H. Tytgat, “Possibility of spontaneous parity violation in hot QCD”, *Phys. Rev. Lett.* **81** (1998) 512–515, arXiv:hep-ph/9804221.
- [7] D. Kharzeev and R. D. Pisarski, “Pionic measures of parity and CP violation in high-energy nuclear collisions”, *Phys. Rev. D* **61** (2000) 111901, arXiv:hep-ph/9906401.
- [8] D. Kharzeev and A. Zhitnitsky, “Charge separation induced by P-odd bubbles in QCD matter”, *Nucl. Phys. A* **797** (2007) 67–79, arXiv:0706.1026 [hep-ph].
- [9] D. E. Kharzeev, L. D. McLerran, and H. J. Warringa, “The Effects of topological charge change in heavy ion collisions: ‘Event by event P and CP violation’”, *Nucl. Phys. A* **803** (2008) 227–253, arXiv:0711.0950 [hep-ph].
- [10] D. E. Kharzeev, “Topology, magnetic field, and strongly interacting matter”, *Ann. Rev. Nucl. Part. Sci.* **65** (2015) 193–214, arXiv:1501.01336 [hep-ph].
- [11] V. Skokov, A. Y. Illarionov, and V. Toneev, “Estimate of the magnetic field strength in heavy-ion collisions”, *Int. J. Mod. Phys. A* **24** (2009) 5925–5932, arXiv:0907.1396 [nucl-th].
- [12] A. Bzdak and V. Skokov, “Event-by-event fluctuations of magnetic and electric fields in heavy ion collisions”, *Phys. Lett. B* **710** (2012) 171–174, arXiv:1111.1949 [hep-ph].
- [13] W.-T. Deng and X.-G. Huang, “Event-by-event generation of electromagnetic fields in heavy-ion collisions”, *Phys. Rev. C* **85** (2012) 044907, arXiv:1201.5108 [nucl-th].
- [14] V. Toneev, V. Voronyuk, E. Bratkovskaya, W. Cassing, V. Konchakovski, and S. Voloshin, “Theoretical analysis of a possible observation of the chiral magnetic effect in Au + Au collisions within the RHIC beam energy scan program”, *Phys. Rev. C* **85** (2012) 034910, arXiv:1112.2595 [hep-ph].
- [15] S. Shi, Y. Jiang, E. Lilleskov, and J. Liao, “Anomalous Chiral Transport in Heavy Ion Collisions from Anomalous-Viscous Fluid Dynamics”, *Annals Phys.* **394** (2018) 50–72, arXiv:1711.02496 [nucl-th].
- [16] K. Fukushima, D. E. Kharzeev, and H. J. Warringa, “The Chiral Magnetic Effect”, *Phys. Rev. D* **78** (2008) 074033, arXiv:0808.3382 [hep-ph].
- [17] D. T. Son and P. Surowka, “Hydrodynamics with Triangle Anomalies”, *Phys. Rev. Lett.* **103** (2009) 191601, arXiv:0906.5044 [hep-th].
- [18] D. E. Kharzeev and H.-U. Yee, “Chiral Magnetic Wave”, *Phys. Rev. D* **83** (2011) 085007, arXiv:1012.6026 [hep-th].
- [19] Y. Burnier, D. E. Kharzeev, J. Liao, and H.-U. Yee, “Chiral magnetic wave at finite baryon density and the electric quadrupole moment of quark-gluon plasma in heavy ion collisions”, *Phys. Rev. Lett.* **107** (2011) 052303, arXiv:1103.1307 [hep-ph].

- [20] D. E. Kharzeev and D. T. Son, “Testing the chiral magnetic and chiral vortical effects in heavy ion collisions”, *Phys. Rev. Lett.* **106** (2011) 062301, arXiv:1010.0038 [hep-ph].
- [21] S. Voloshin and Y. Zhang, “Flow study in relativistic nuclear collisions by Fourier expansion of azimuthal particle distributions”, *Z. Phys.* **C70** (1996) 665–672, arXiv:hep-ph/9407282.
- [22] A. M. Poskanzer and S. A. Voloshin, “Methods for analyzing anisotropic flow in relativistic nuclear collisions”, *Phys. Rev. C* **58** (1998) 1671–1678, arXiv:nucl-ex/9805001.
- [23] R. S. Bhalerao and J.-Y. Ollitrault, “Eccentricity fluctuations and elliptic flow at RHIC”, *Phys. Lett. B* **641** (2006) 260–264, arXiv:nucl-th/0607009.
- [24] **PHOBOS** Collaboration, B. Alver *et al.*, “Importance of correlations and fluctuations on the initial source eccentricity in high-energy nucleus-nucleus collisions”, *Phys. Rev. C* **77** (2008) 014906, arXiv:0711.3724 [nucl-ex].
- [25] B. Alver and G. Roland, “Collision geometry fluctuations and triangular flow in heavy-ion collisions”, *Phys. Rev. C* **81** (2010) 054905, arXiv:1003.0194 [nucl-th]. [Erratum: *Phys.Rev.C* 82, 039903 (2010)].
- [26] **PHOBOS** Collaboration, S. Manly *et al.*, “System size, energy and pseudorapidity dependence of directed and elliptic flow at RHIC”, *Nucl. Phys. A* **774** (2006) 523–526, arXiv:nucl-ex/0510031.
- [27] S. A. Voloshin, “Parity violation in hot QCD: How to detect it”, *Phys. Rev.* **C70** (2004) 057901, arXiv:hep-ph/0406311.
- [28] **STAR** Collaboration, B. I. Abelev *et al.*, “Azimuthal Charged-Particle Correlations and Possible Local Strong Parity Violation”, *Phys. Rev. Lett.* **103** (2009) 251601, arXiv:0909.1739 [nucl-ex].
- [29] **STAR** Collaboration, B. I. Abelev *et al.*, “Observation of charge-dependent azimuthal correlations and possible local strong parity violation in heavy ion collisions”, *Phys. Rev. C* **81** (2010) 054908, arXiv:0909.1717 [nucl-ex].
- [30] **STAR** Collaboration, L. Adamczyk *et al.*, “Fluctuations of charge separation perpendicular to the event plane and local parity violation in $\sqrt{s_{NN}} = 200$ GeV Au+Au collisions at the BNL Relativistic Heavy Ion Collider”, *Phys. Rev. C* **88** (2013) 064911, arXiv:1302.3802 [nucl-ex].
- [31] **STAR** Collaboration, L. Adamczyk *et al.*, “Beam-energy dependence of charge separation along the magnetic field in Au+Au collisions at RHIC”, *Phys. Rev. Lett.* **113** (2014) 052302, arXiv:1404.1433 [nucl-ex].
- [32] **STAR** Collaboration, L. Adamczyk *et al.*, “Measurement of charge multiplicity asymmetry correlations in high-energy nucleus-nucleus collisions at $\sqrt{s_{NN}} = 200$ GeV”, *Phys. Rev. C* **89** (2014) 044908, arXiv:1303.0901 [nucl-ex].
- [33] **STAR** Collaboration, J. Adam *et al.*, “Charge-dependent pair correlations relative to a third particle in $p + Au$ and $d + Au$ collisions at RHIC”, *Phys. Lett. B* **798** (2019) 134975, arXiv:1906.03373 [nucl-ex].
- [34] **STAR** Collaboration, M. S. Abdallah *et al.*, “Pair invariant mass to isolate background in the search for the chiral magnetic effect in Au + Au collisions at $\sqrt{s_{NN}} = 200$ GeV”, *Phys. Rev. C* **106** (2022) 034908, arXiv:2006.05035 [nucl-ex].

- [35] **STAR** Collaboration, M. S. Abdallah *et al.*, “Search for the Chiral Magnetic Effect via Charge-Dependent Azimuthal Correlations Relative to Spectator and Participant Planes in Au + Au Collisions at $\sqrt{s_{NN}} = 200$ GeV”, *Phys. Rev. Lett.* **128** (2022) 092301, arXiv:2106.09243 [nucl-ex].
- [36] **ALICE** Collaboration, B. Abelev *et al.*, “Charge separation relative to the reaction plane in Pb–Pb collisions at $\sqrt{s_{NN}} = 2.76$ TeV”, *Phys. Rev. Lett.* **110** (2013) 012301, arXiv:1207.0900 [nucl-ex].
- [37] **ALICE** Collaboration, S. Acharya *et al.*, “Constraining the Chiral Magnetic Effect with charge-dependent azimuthal correlations in Pb–Pb collisions at $\sqrt{s_{NN}} = 2.76$ and 5.02 TeV”, *JHEP* **09** (2020) 160, arXiv:2005.14640 [nucl-ex].
- [38] **CMS** Collaboration, V. Khachatryan *et al.*, “Observation of charge-dependent azimuthal correlations in p –Pb collisions and its implication for the search for the chiral magnetic effect”, *Phys. Rev. Lett.* **118** (2017) 122301, arXiv:1610.00263 [nucl-ex].
- [39] **CMS** Collaboration, A. M. Sirunyan *et al.*, “Constraints on the chiral magnetic effect using charge-dependent azimuthal correlations in p Pb and PbPb collisions at the CERN Large Hadron Collider”, *Phys. Rev. C* **97** (2018) 044912, arXiv:1708.01602 [nucl-ex].
- [40] F. Wang, “Effects of Cluster Particle Correlations on Local Parity Violation Observables”, *Phys. Rev. C* **81** (2010) 064902, arXiv:0911.1482 [nucl-ex].
- [41] A. Bzdak, V. Koch, and J. Liao, “Remarks on possible local parity violation in heavy ion collisions”, *Phys. Rev. C* **81** (2010) 031901, arXiv:0912.5050 [nucl-th].
- [42] J. Liao, V. Koch, and A. Bzdak, “On the Charge Separation Effect in Relativistic Heavy Ion Collisions”, *Phys. Rev. C* **82** (2010) 054902, arXiv:1005.5380 [nucl-th].
- [43] S. Schlichting and S. Pratt, “Charge conservation at energies available at the BNL Relativistic Heavy Ion Collider and contributions to local parity violation observables”, *Phys. Rev. C* **83** (2011) 014913, arXiv:1009.4283 [nucl-th].
- [44] **ALICE** Collaboration, S. Acharya *et al.*, “Search for the Chiral Magnetic Effect with charge-dependent azimuthal correlations in Xe–Xe collisions at $\sqrt{s_{NN}} = 5.44$ TeV”, *Phys. Lett. B* **856** (2024) 138862, arXiv:2210.15383 [nucl-ex].
- [45] W.-Y. Wu *et al.*, “Global constraint on the magnitude of anomalous chiral effects in heavy-ion collisions”, *Phys. Rev. C* **107** (2023) L031902, arXiv:2211.15446 [nucl-th].
- [46] P. Christakoglou, S. Qiu, and J. Staa, “Systematic study of the chiral magnetic effect with the AVFD model at LHC energies”, *Eur. Phys. J. C* **81** (2021) 717, arXiv:2106.03537 [nucl-th].
- [47] J. Schukraft, A. Timmins, and S. A. Voloshin, “Ultra-relativistic nuclear collisions: event shape engineering”, *Phys. Lett.* **B719** (2013) 394–398, arXiv:1208.4563 [nucl-ex].
- [48] **STAR** Collaboration, M. Abdallah *et al.*, “Search for the chiral magnetic effect with isobar collisions at $\sqrt{s_{NN}} = 200$ GeV by the STAR Collaboration at the BNL Relativistic Heavy Ion Collider”, *Phys. Rev. C* **105** (2022) 014901, arXiv:2109.00131 [nucl-ex].
- [49] **STAR** Collaboration, M. I. Abdulhamid *et al.*, “Upper limit on the chiral magnetic effect in isobar collisions at the Relativistic Heavy-Ion Collider”, *Phys. Rev. Res.* **6** (2024) L032005, arXiv:2308.16846 [nucl-ex].

- [50] H.-j. Xu, J. Zhao, X. Wang, H. Li, Z.-W. Lin, C. Shen, and F. Wang, “Varying the chiral magnetic effect relative to flow in a single nucleus-nucleus collision”, *Chin. Phys. C* **42** (2018) 084103, arXiv:1710.07265 [nucl-th].
- [51] S. A. Voloshin, “Estimate of the signal from the chiral magnetic effect in heavy-ion collisions from measurements relative to the participant and spectator flow planes”, *Phys. Rev. C* **98** (2018) 054911, arXiv:1805.05300 [nucl-ex].
- [52] ALICE Collaboration, S. Acharya *et al.*, “Constraining the magnitude of the Chiral Magnetic Effect with Event Shape Engineering in Pb–Pb collisions at $\sqrt{s_{NN}} = 2.76$ TeV”, *Phys. Lett.* **B777** (2018) 151–162, arXiv:1709.04723 [nucl-ex].
- [53] STAR Collaboration, B. E. Aboona *et al.*, “Search for the chiral magnetic effect through beam energy dependence of charge separation using event shape selection”, *Phys. Rev. C* (2025) –. <https://link.aps.org/doi/10.1103/pj7s-9ym7>.
- [54] ALICE Collaboration, K. Aamodt *et al.*, “The ALICE experiment at the CERN LHC”, *JINST* **3** (2008) S08002.
- [55] ALICE Collaboration, B. B. Abelev *et al.*, “Performance of the ALICE Experiment at the CERN LHC”, *Int. J. Mod. Phys. A* **29** (2014) 1430044, arXiv:1402.4476 [nucl-ex].
- [56] ALICE Collaboration, K. Aamodt *et al.*, “Alignment of the ALICE Inner Tracking System with cosmic-ray tracks”, *JINST* **5** (2010) P03003, arXiv:1001.0502 [physics.ins-det].
- [57] J. Alme *et al.*, “The ALICE TPC, a large 3-dimensional tracking device with fast readout for ultra-high multiplicity events”, *Nucl. Instrum. Meth. A* **622** (2010) 316–367, arXiv:1001.1950 [physics.ins-det].
- [58] ALICE Collaboration, E. Abbas *et al.*, “Performance of the ALICE VZERO system”, *JINST* **8** (2013) P10016, arXiv:1306.3130 [nucl-ex].
- [59] ALICE Collaboration, B. Abelev *et al.*, “Centrality determination of Pb–Pb collisions at $\sqrt{s_{NN}} = 2.76$ TeV with ALICE”, *Phys. Rev. C* **88** (2013) 044909, arXiv:1301.4361 [nucl-ex].
- [60] R. Arnaldi *et al.*, “The zero degree calorimeters for the ALICE experiment”, *Nucl. Instrum. Meth. A* **581** (2007) 397–401. [Erratum: *Nucl.Instrum.Meth.A* 604, 765 (2009)].
- [61] ALICE Collaboration, J. Adam *et al.*, “Anisotropic flow of charged particles in Pb–Pb collisions at $\sqrt{s_{NN}} = 5.02$ TeV”, *Phys. Rev. Lett.* **116** (2016) 132302, arXiv:1602.01119 [nucl-ex].
- [62] STAR Collaboration, C. Adler *et al.*, “Elliptic flow from two and four particle correlations in Au+Au collisions at $\sqrt{s_{NN}} = 130$ GeV”, *Phys. Rev. C* **66** (2002) 034904, arXiv:nucl-ex/0206001.
- [63] ALICE Collaboration, B. Abelev *et al.*, “Directed Flow of Charged Particles at Midrapidity Relative to the Spectator Plane in Pb–Pb Collisions at $\sqrt{s_{NN}}=2.76$ TeV”, *Phys. Rev. Lett.* **111** (2013) 232302, arXiv:1306.4145 [nucl-ex].
- [64] R. Barlow, “Systematic errors: Facts and fictions”, in *Conference on Advanced Statistical Techniques in Particle Physics*, pp. 134–144. 7, 2002. arXiv:hep-ex/0207026.
- [65] ALICE Collaboration, S. Acharya *et al.*, “Elliptic flow of charged particles at midrapidity relative to the spectator plane in Pb–Pb and Xe–Xe collisions”, *Phys. Lett. B* **846** (2023) 137453, arXiv:2204.10240 [nucl-ex].

- [66] W. Broniowski, P. Bozek, and M. Rybczynski, “Fluctuating initial conditions in heavy-ion collisions from the Glauber approach”, *Phys. Rev. C* **76** (2007) 054905, arXiv:0706.4266 [nucl-th].
- [67] H.-J. Drescher and Y. Nara, “Eccentricity fluctuations from the color glass condensate at RHIC and LHC”, *Phys. Rev. C* **76** (2007) 041903, arXiv:0707.0249 [nucl-th].
- [68] ALICE Collaboration, J. Adam *et al.*, “Event shape engineering for inclusive spectra and elliptic flow in Pb–Pb collisions at $\sqrt{s_{NN}} = 2.76$ TeV”, *Phys. Rev. C* **93** (2016) 034916, arXiv:1507.06194 [nucl-ex].
- [69] F. G. Gardim, F. Grassi, M. Luzum, and J.-Y. Ollitrault, “Mapping the hydrodynamic response to the initial geometry in heavy-ion collisions”, *Phys. Rev. C* **85** (2012) 024908, arXiv:1111.6538 [nucl-th].
- [70] M. L. Miller, K. Reygers, S. J. Sanders, and P. Steinberg, “Glauber modeling in high energy nuclear collisions”, *Ann. Rev. Nucl. Part. Sci.* **57** (2007) 205–243, arXiv:nucl-ex/0701025.
- [71] ALICE Collaboration, S. Acharya *et al.*, “The ALICE experiment: a journey through QCD”, *Eur. Phys. J. C* **84** (2024) 813, arXiv:2211.04384 [nucl-ex].
- [72] ALICE Collaboration, S. Acharya *et al.*, “Anisotropic flow in Xe–Xe collisions at $\sqrt{s_{NN}} = 5.44$ TeV”, *Phys. Lett. B* **784** (2018) 82–95, arXiv:1805.01832 [nucl-ex].
- [73] J. S. Moreland, J. E. Bernhard, and S. A. Bass, “Alternative ansatz to wounded nucleon and binary collision scaling in high-energy nuclear collisions”, *Phys. Rev. C* **92** (2015) 011901, arXiv:1412.4708 [nucl-th].
- [74] ALICE Collaboration, S. Acharya *et al.*, “Anisotropic flow in Xe–Xe collisions at $\sqrt{s_{NN}} = 5.44$ TeV”, *Phys. Lett. B* **784** (2018) 82–95, arXiv:1805.01832 [nucl-ex].
- [75] ALICE Collaboration, S. Acharya *et al.*, “Constraining the Chiral Magnetic Effect with charge-dependent azimuthal correlations in Pb–Pb collisions at $\sqrt{s_{NN}} = 2.76$ and 5.02 TeV”, *JHEP* **09** (2020) 160, arXiv:2005.14640 [nucl-ex].
- [76] Z. Citron *et al.*, “Report from Working Group 5: Future physics opportunities for high-density QCD at the LHC with heavy-ion and proton beams”, *CERN Yellow Rep. Monogr.* **7** (2019) 1159–1410, arXiv:1812.06772 [hep-ph].
- [77] P. Christakoglou, “Probing the magnetic field strength dependence of the chiral magnetic effect”, *Eur. Phys. J. C* **84** (2024) 290, arXiv:2308.02361 [nucl-th].

A The ALICE Collaboration

D.A.H. Abdallah ¹³⁴, I.J. Abualrob ¹¹², S. Acharya ⁴⁹, K. Agarwal ^{II,23}, G. Aglieri Rinella ³², L. Aglietta ²⁴, N. Agrawal ²⁵, Z. Ahammed ¹³², S. Ahmad ¹⁵, I. Ahuja ³⁶, Z. Akbar ⁷⁹, V. Akishina ³⁸, M. Al-Turany ⁹⁴, B. Alessandro ⁵⁵, R. Alfaro Molina ⁶⁶, B. Ali ¹⁵, A. Alici ^{I,25}, J. Alme ²⁰, G. Alocco ²⁴, T. Alt ⁶³, I. Altsybeev ⁹², C. Andrei ⁴⁴, N. Andreou ¹¹¹, A. Andronic ¹²³, M. Angeletti ³², V. Anguelov ⁹¹, F. Antinori ⁵³, P. Antonioli ⁵⁰, N. Apadula ⁷¹, H. Appelshäuser ⁶³, S. Arcelli ^{I,25}, R. Arnaldi ⁵⁵, I.C. Arsene ¹⁹, M. Arslandok ¹³⁵, A. Augustinus ³², R. Averbeck ⁹⁴, M.D. Azmi ¹⁵, H. Baba ¹²¹, A.R.J. Babu ¹³⁴, A. Badalà ⁵², J. Bae ¹⁰⁰, Y. Bae ¹⁰⁰, Y.W. Baek ¹⁰⁰, X. Bai ¹¹⁶, R. Bailhache ⁶³, Y. Bailung ¹²⁵, R. Bala ⁸⁸, A. Baldisseri ¹²⁷, B. Balis ², S. Bangalia ¹¹⁴, Z. Banoo ⁸⁸, V. Barbasova ³⁶, F. Barile ³¹, L. Barioglio ⁵⁵, M. Barlou ²⁴, B. Barman ⁴⁰, G.G. Barnaföldi ⁴⁵, L.S. Barnby ¹¹¹, E. Barreau ⁹⁹, V. Barret ¹²⁴, L. Barreto ¹⁰⁶, K. Barth ³², E. Bartsch ⁶³, N. Bastid ¹²⁴, G. Batigne ⁹⁹, D. Battistini ^{34,92}, B. Batyunya ¹³⁹, L. Baudino ²⁴, D. Bauri ⁴⁶, J.L. Bazo Alba ⁹⁸, I.G. Bearden ⁸⁰, P. Becht ⁹⁴, D. Behera ^{77,47}, S. Behera ⁴⁶, I. Belikov ¹²⁶, V.D. Bella ¹²⁶, F. Bellini ²⁵, R. Bellwied ¹¹², L.G.E. Beltran ¹⁰⁵, Y.A.V. Beltran ⁴³, G. Bencedi ⁴⁵, O. Benchikhi ⁷³, A. Bensaoula ¹¹², S. Beole ²⁴, A. Berdnikova ⁹¹, L. Bergmann ⁷¹, L. Bernardinis ²³, L. Betev ³², P.P. Bhaduri ¹³², T. Bhalla ⁸⁷, A. Bhasin ⁸⁸, B. Bhattacharjee ⁴⁰, L. Bianchi ²⁴, J. Bielčik ³⁴, J. Bielčíková ⁸³, A. Bilandzic ⁹², A. Binoy ¹¹⁴, G. Biro ⁴⁵, S. Biswas ⁴, M.B. Blidaru ⁹⁴, N. Bluhme ³⁸, C. Blume ⁶³, F. Bock ⁸⁴, T. Bodova ²⁰, L. Boldizsár ⁴⁵, M. Bombara ³⁶, P.M. Bond ³², G. Bonomi ^{131,54}, H. Borel ¹²⁷, A. Borissov ¹³⁹, A.G. Borquez Carcamo ⁹¹, E. Botta ²⁴, N. Bouchhar ¹⁷, Y.E.M. Bouziani ⁶³, D.C. Brandibur ⁶², L. Bratrud ⁶³, P. Braun-Munzinger ⁹⁴, M. Bregant ¹⁰⁶, M. Broz ³⁴, G.E. Bruno ^{93,31}, V.D. Buchakchiev ³⁵, M.D. Buckland ⁸², H. Buesching ⁶³, S. Bufalino ²⁹, P. Buhler ⁷³, N. Burmasov ¹³⁹, Z. Buthelezi ^{67,120}, A. Bylinkin ²⁰, C. Carr ⁹⁷, J.C. Cabanillas Noris ¹⁰⁵, M.F.T. Cabrera ¹¹², H. Caines ¹³⁵, A. Caliva ²⁸, E. Calvo Villar ⁹⁸, J.M.M. Camacho ¹⁰⁵, P. Camerini ²³, M.T. Camerlingo ⁴⁹, F.D.M. Canedo ¹⁰⁶, S. Cannito ²³, S.L. Cantway ¹³⁵, M. Carabas ¹⁰⁹, F. Carnesecchi ³², L.A.D. Carvalho ¹⁰⁶, J. Castillo Castellanos ¹²⁷, M. Castoldi ³², F. Catalano ¹¹², S. Cattaruzzi ²³, R. Cerri ²⁴, I. Chakaberia ⁷¹, P. Chakraborty ¹³³, J.W.O. Chan ¹¹², S. Chandra ¹³², S. Chapeland ³², M. Chartier ¹¹⁵, S. Chattopadhyay ¹³², M. Chen ³⁹, T. Cheng ⁶, M.I. Cherciu ⁶², C. Cheshkov ¹²⁵, D. Chiappara ²⁷, V. Chibante Barroso ³², D.D. Chinellato ⁷³, F. Chinu ²⁴, E.S. Chizzali ^{III,92}, J. Cho ⁵⁷, S. Cho ⁵⁷, P. Chochula ³², Z.A. Chochulska ^{IV,133}, P. Christakoglou ⁸¹, P. Christiansen ⁷², T. Chujo ¹²², B. Chytla ¹³³, M. Ciacco ²⁴, C. Cicalo ⁵¹, G. Cimator ^{32,24}, F. Cindolo ⁵⁰, F. Colamaria ⁴⁹, D. Colella ³¹, A. Colelli ³¹, M. Colocci ²⁵, M. Concas ³², G. Conesa Balbastre ⁷⁰, Z. Conesa del Valle ¹²⁸, G. Contin ²³, J.G. Contreras ³⁴, M.L. Coquet ⁹⁹, P. Cortese ^{130,55}, M.R. Cosentino ¹⁰⁸, F. Costa ³², S. Costanza ²¹, P. Crochet ¹²⁴, M.M. Czarnynoga ¹³³, A. Dainese ⁵³, E. Dall'occo ³², G. Dange ³⁸, M.C. Danisch ¹⁶, A. Danu ⁶², A. Daribayeva ³⁸, P. Das ³², S. Das ⁴, A.R. Dash ¹²³, S. Dash ⁴⁶, A. De Caro ²⁸, G. de Cataldo ⁴⁹, J. de Cuveland ³⁸, A. De Falco ²², D. De Gruttola ²⁸, N. De Marco ⁵⁵, C. De Martin ²³, S. De Pasquale ²⁸, R. Deb ¹³¹, R. Del Grande ³⁴, L. Dello Stritto ³², G.G.A. de Souza ^{V,106}, P. Dhankeer ¹⁸, D. Di Bari ³¹, M. Di Costanzo ²⁹, A. Di Mauro ³², B. Di Ruzza ^{I,129,49}, B. Diab ³², Y. Ding ⁶, J. Ditzel ⁶³, R. Divià ³², U. Dmitrieva ⁵⁵, A. Dobrin ⁶², B. Dönigus ⁶³, L. Döpper ⁴¹, L. Drzensla ², J.M. Dubinski ¹³³, A. Dubla ⁹⁴, P. Dupieux ¹²⁴, N. Dzalaiova ¹³, T.M. Eder ¹²³, R.J. Ehlers ⁷¹, F. Eisenhut ⁶³, R. Ejima ⁸⁹, D. Elia ⁴⁹, B. Erazmus ⁹⁹, F. Ercolessi ²⁵, B. Espagnon ¹²⁸, G. Eulisse ³², D. Evans ⁹⁷, L. Fabbietti ⁹², G. Fabbri ⁵⁰, M. Faggin ³², J. Faivre ⁷⁰, W. Fan ¹¹², T. Fang ⁶, A. Fantoni ⁴⁸, A. Feliciello ⁵⁵, W. Feng ⁶, A. Fernández Téllez ⁴³, B. Fernando ¹³⁴, L. Ferrandi ¹⁰⁶, A. Ferrero ¹²⁷, C. Ferrero ^{VI,55}, A. Ferretti ²⁴, D. Finogeev ¹³⁹, F.M. Fionda ⁵¹, A.N. Flores ¹⁰⁴, S. Foertsch ⁶⁷, I. Fokin ⁹¹, U. Follo ^{VI,55}, R. Forynski ¹¹¹, E. Fragiaco ⁵⁶, H. Fribert ⁹², U. Fuchs ³², D. Fuligno ²³, N. Funicello ²⁸, C. Furget ⁷⁰, A. Furs ¹³⁹, T. Fusayasu ⁹⁵, J.J. Gaardhøje ⁸⁰, M. Gagliardi ²⁴, A.M. Gago ⁹⁸, T. Gahlaut ⁴⁶, C.D. Galvan ¹⁰⁵, S. Gami ⁷⁷, C. Garabatos ⁹⁴, J.M. Garcia ⁴³, E. Garcia-Solis ⁹, S. Garetti ¹²⁸, C. Gargiulo ³², P. Gasik ⁹⁴, A. Gautam ¹¹⁴, M.B. Gay Ducati ⁶⁵, M. Germain ⁹⁹, R.A. Gernhaeuser ⁹², M. Giacalone ³², G. Gioachin ²⁹, S.K. Giri ¹³², P. Giubellino ⁵⁵, P. Giubilato ²⁷, P. Glässel ⁹¹, E. Glimos ¹¹⁹, M.G.F.S.A. Gomes ⁹¹, L. Gonella ²³, V. Gonzalez ¹³⁴, M. Gorgon ², K. Goswami ⁴⁷, S. Gotovac ³³, V. Grabski ⁶⁶, L.K. Graczykowski ¹³³, E. Grecka ⁸³, A. Grelli ⁵⁸, C. Grigoras ³², S. Grigoryan ^{139,1}, O.S. Groettvik ³², M. Gronbeck ⁴¹, F. Grosa ³², S. Gross-Böling ⁹⁴, J.F. Grosse-Oetringhaus ³², R. Grosso ⁹⁴, D. Grund ³⁴, N.A. Grunwald ⁹¹, R. Guernano ⁷⁰, M. Guilbaud ⁹⁹, K. Gulbrandsen ⁸⁰, J.K. Gumprecht ⁷³, T. Gündem ⁶³, T. Gunji ¹²¹, J. Guo ¹⁰, W. Guo ⁶, A. Gupta ⁸⁸, R. Gupta ⁸⁸, R. Gupta ⁴⁷, K. Gwizdziel ¹³³, L. Gyulai ⁴⁵, T. Hachiya ⁷⁵, C. Hadjidakis ¹²⁸, F.U. Haider ⁸⁸,

S. Haidlova³⁴, M. Haldar⁴, W. Ham¹⁰⁰, H. Hamagaki⁷⁴, Y. Han¹³⁷, R. Hannigan¹⁰⁴, J. Hansen⁷², J.W. Harris¹³⁵, A. Harton⁹, M.V. Hartung⁶³, A. Hasan¹¹⁸, H. Hassan¹¹³, D. Hatzifotiadiou⁵⁰, P. Hauer⁴¹, L.B. Havener¹³⁵, E. Hellbär³², H. Helstrup³⁷, M. Hemmer⁶³, S.G. Hernandez¹¹², G. Herrera Corral⁸, K.F. Hetland³⁷, B. Heybeck⁶³, H. Hillemanns³², B. Hippolyte¹²⁶, I.P.M. Hobus⁸¹, F.W. Hoffmann³⁸, B. Hofman⁵⁸, Y. Hong⁵⁷, A. Horzyk², Y. Hou^{94,11}, P. Hristov³², L.M. Huhta¹¹³, T.J. Humanic⁸⁵, V. Humlova³⁴, M. Husar⁸⁶, A. Hutson¹¹², D. Hutter³⁸, M.C. Hwang¹⁸, M. Inaba¹²², A. Isakov⁸¹, T. Isidori¹¹⁴, M.S. Islam⁴⁶, M. Ivanov⁹⁴, M. Ivanov¹³, K.E. Iversen⁷², J.G. Kim¹³⁷, M. Jablonski², B. Jacak^{18,71}, N. Jacazio²⁵, P.M. Jacobs⁷¹, A. Jadlovska¹⁰², S. Jadlovska¹⁰², S. Jaelani⁷⁹, C. Jahnke¹⁰⁷, M.J. Jakubowska¹³³, E.P. Jamro², D.M. Janik³⁴, M.A. Janik¹³³, S. Ji¹⁶, Y. Ji⁹⁴, S. Jia⁸⁰, T. Jiang¹⁰, A.A.P. Jimenez⁶⁴, S. Jin¹⁰, F. Jonas⁷¹, D.M. Jones¹¹⁵, J.M. Jowett^{32,94}, J. Jung⁶³, M. Jung⁶³, A. Junique³², J. Juracka³⁴, J. Kaewjai^{115,101}, A. Kaiser^{32,94}, P. Kalinak⁵⁹, A. Kalweit³², A. Karasu Uysal¹³⁶, N. Karatzenis⁹⁷, T. Karavicheva¹³⁹, M.J. Karwowska¹³³, V. Kashyap⁷⁷, M. Keil³², B. Ketzer⁴¹, J. Keul⁶³, S.S. Khade⁴⁷, A. Khuntia⁵⁰, Z. Khuranova⁶³, B. Kileng³⁷, B. Kim¹⁰⁰, D.J. Kim¹¹³, D. Kim¹⁰⁰, E.J. Kim⁶⁸, G. Kim⁵⁷, H. Kim⁵⁷, J. Kim¹³⁷, J. Kim⁵⁷, J. Kim³², M. Kim¹⁸, S. Kim¹⁷, T. Kim¹³⁷, J.T. Kinner¹²³, I. Kisel³⁸, A. Kisiel¹³³, J.L. Klay⁵, J. Klein³², S. Klein⁷¹, C. Klein-Bösing¹²³, M. Kleiner⁶³, A. Kluge³², M.B. Knuesel¹³⁵, C. Kobdaj¹⁰¹, R. Kohara¹²¹, A. Kondratyev¹³⁹, J. Konig⁶³, P.J. Konopka³², G. Kornakov¹³³, M. Korwieser⁹², C. Koster⁸¹, A. Kotliarov⁸³, N. Kovacic⁸⁶, M. Kowalski¹⁰³, V. Kozuharov³⁵, G. Kozlov³⁸, I. Králik⁵⁹, A. Kravčáková³⁶, M.A. Krawczyk³², L. Krcal³², F. Krizek⁸³, K. Krizkova Gajdosova³⁴, C. Krug⁶⁵, M. Krüger⁶³, E. Kryshen¹³⁹, V. Kučera⁵⁷, C. Kuhn¹²⁶, D. Kumar¹³², L. Kumar⁸⁷, N. Kumar⁸⁷, S. Kumar⁴⁹, S. Kundu³², M. Kuo¹²², P. Kurashvili⁷⁶, S. Kurita⁸⁹, S. Kushpil⁸³, A. Kuznetsov¹³⁹, M.J. Kweon⁵⁷, Y. Kwon¹³⁷, S.L. La Pointe³⁸, P. La Rocca²⁶, A. Lakrathok¹⁰¹, S. Lambert⁹⁹, A.R. Landou⁷⁰, R. Langoy¹¹⁸, P. Larionov³², E. Laudi³², L. Lautner⁹², R.A.N. Laveaga¹⁰⁵, R. Lavicka⁷³, R. Lea^{131,54}, J.B. Lebert³⁸, H. Lee¹⁰⁰, S. Lee⁵⁷, I. Legrand⁴⁴, G. Legras¹²³, A.M. Lejeune³⁴, T.M. Lelek², I. León Monzón¹⁰⁵, M.M. Lesch⁹², P. Lévai⁴⁵, M. Li⁶, P. Li¹⁰, X. Li¹⁰, B.E. Liang-Gilman¹⁸, J. Lien¹¹⁸, R. Lietava⁹⁷, I. Likmeta¹¹², B. Lim⁵⁵, H. Lim¹⁶, S.H. Lim¹⁶, Y.N. Lima¹⁰⁶, S. Lin¹⁰, V. Lindenstruth³⁸, C. Lippmann⁹⁴, D. Liskova¹⁰², D.H. Liu⁶, J. Liu¹¹⁵, Y. Liu⁶, G.S.S. Liveraro¹⁰⁷, I.M. Lofnes²⁰, C. Loizides²⁰, S. Lokos¹⁰³, J. Lömker⁵⁸, X. Lopez¹²⁴, E. López Torres⁷, C. Lotteau¹²⁵, P. Lu¹¹⁶, W. Lu⁶, Z. Lu¹⁰, O. Lubyets⁹⁴, G.A. Lucia²⁹, F.V. Lugo⁶⁶, J. Luo³⁹, G. Luparello⁵⁶, J. M. Friedrich⁹², Y.G. Ma³⁹, V. Machacek⁸⁰, M. Mager³², M. Mahlein⁹², A. Maire¹²⁶, E. Majerz², M.V. Makariev³⁵, G. Malfattore⁵⁰, N.M. Malik⁸⁸, N. Malik¹⁵, D. Mallick¹²⁸, N. Mallick¹¹³, G. Mandaglio^{30,52}, S. Mandal⁷⁷, S.K. Mandal⁷⁶, A. Manea⁶², R. Manhart⁹², A.K. Manna⁴⁷, F. Manso¹²⁴, G. Mantzaridis⁹², V. Manzari⁴⁹, Y. Mao⁶, R.W. Marcjan², G.V. Margagliotti²³, A. Margotti⁵⁰, A. Marín⁹⁴, C. Markert¹⁰⁴, P. Martinengo³², M.I. Martínez⁴³, M.P.P. Martins^{32,106}, S. Masciocchi⁹⁴, M. Masera²⁴, A. Masoni⁵¹, L. Massacrier¹²⁸, O. Massen⁵⁸, A. Mastroserio^{129,49}, L. Mattei^{24,124}, S. Mattiazzo²⁷, A. Matyja¹⁰³, J.L. Mayo¹⁰⁴, F. Mazzaschi³², M. Mazzilli³¹, Y. Melikyan⁴², M. Melo¹⁰⁶, A. Menchaca-Rocha⁶⁶, J.E.M. Mendez⁶⁴, E. Meninno⁷³, M.W. Menzel^{32,91}, M. Meres¹³, L. Micheletti⁵⁵, D. Mihai¹⁰⁹, D.L. Mihaylov⁹², A.U. Mikalsen²⁰, K. Mikhaylov¹³⁹, L. Millot⁷⁰, N. Minafra¹¹⁴, D. Miśkowiec⁹⁴, A. Modak⁵⁶, B. Mohanty⁷⁷, M. Mohisin Khan^{VII,15}, M.A. Molander⁴², M.M. Mondal⁷⁷, S. Monira¹³³, D.A. Moreira De Godoy¹²³, A. Morsch³², C. Moscatelli²³, T. Mrnjavac³², S. Mrozinski⁶³, V. Muccifora⁴⁸, S. Muhuri¹³², A. Mulliri²², M.G. Munhoz¹⁰⁶, R.H. Munzer⁶³, L. Musa³², J. Musinsky⁵⁹, J.W. Myrcha¹³³, B. Naik¹²⁰, A.I. Nambrath¹⁸, B.K. Nandi⁴⁶, R. Nania⁵⁰, E. Nappi⁴⁹, A.F. Nassirpour¹⁷, V. Nastase¹⁰⁹, A. Nath⁹¹, N.F. Nathanson⁸⁰, A. Neagu¹⁹, L. Nellen⁶⁴, R. Nepeivoda⁷², S. Nese¹⁹, N. Nicassio³¹, B.S. Nielsen⁸⁰, E.G. Nielsen⁸⁰, F. Noferini⁵⁰, S. Noh¹², P. Nomokonov¹³⁹, J. Norman¹¹⁵, N. Novitzky⁸⁴, J. Nystrand²⁰, M.R. Ockleton¹¹⁵, M. Ogino⁷⁴, J. Oh¹⁶, S. Oh¹⁷, A. Ohlson⁷², M. Oida⁸⁹, L.A.D. Oliveira^{I,107}, C. Oppedisano⁵⁵, A. Ortiz Velasquez⁶⁴, H. Osanai⁷⁴, J. Otwinowski¹⁰³, M. Oya⁸⁹, K. Oyama⁷⁴, S. Padhan^{131,46}, D. Pagano^{131,54}, V. Pagliarino⁵⁵, G. Paić⁶⁴, A. Palasciano^{93,49}, I. Panasenکو⁷², P. Panigrahi⁴⁶, C. Pantouvakis²⁷, H. Park¹²², J. Park¹²², S. Park¹⁰⁰, T.Y. Park¹³⁷, J.E. Parkkila¹³³, P.B. Pati⁸⁰, Y. Patley⁴⁶, R.N. Patra⁴⁹, J. Patter⁴⁷, B. Paul¹³², F. Pazdic⁹⁷, H. Pei⁶, T. Peitzmann⁵⁸, X. Peng^{53,11}, S. Perciballi²⁴, G.M. Perez⁷, M. Petrovici⁴⁴, S. Piano⁵⁶, M. Pikna¹³, P. Pillot⁹⁹, O. Pinazza^{50,32}, C. Pinto³², S. Pisano⁴⁸, M. Płoskoń⁷¹, A. Plachta¹³³, M. Planinic⁸⁶, D.K. Plociennik², S. Politano³², N. Poljak⁸⁶, A. Pop⁴⁴, S. Porteboeuf-Houssais¹²⁴, J.S. Potgieter¹¹⁰, I.Y. Pozos⁴³, K.K. Pradhan⁴⁷, S.K. Prasad⁴, S. Prasad⁴⁷, R. Preghenella⁵⁰,

F. Prino ⁵⁵, C.A. Pruneau ¹³⁴, M. Puccio ³², S. Pucillo ²⁸, S. Pulawski ¹¹⁷, L. Quaglia ²⁴,
A.M.K. Radhakrishnan ⁴⁷, S. Ragoni ¹⁴, A. Rai ¹³⁵, A. Rakotozafindrabe ¹²⁷, N. Ramasubramanian ¹²⁵,
L. Ramello ^{130,55}, C.O. Ramírez-Álvarez ⁴³, M. Rasa ²⁶, S.S. Räsänen ⁴², R. Rath ⁹⁴, M.P. Rauch ²⁰,
I. Ravasenga ³², M. Razza ²⁵, K.F. Read ^{84,119}, C. Reckziegel ¹⁰⁸, A.R. Redelbach ³⁸,
K. Redlich ^{VIII,76}, C.A. Reetz ⁹⁴, H.D. Regules-Medel ⁴³, A. Rehman ²⁰, F. Reidt ³²,
H.A. Reme-Ness ³⁷, K. Reygers ⁹¹, M. Richter ²⁰, A.A. Riedel ⁹², W. Riegler ³², A.G. Riffero ²⁴,
M. Rignanese ²⁷, C. Ripoli ²⁸, C. Ristea ⁶², M.V. Rodriguez ³², M. Rodríguez Cahuantzi ⁴³,
K. Røed ¹⁹, E. Rogochaya ¹³⁹, D. Rohr ³², D. Röhrich ²⁰, S. Rojas Torres ³⁴, P.S. Rokita ¹³³,
G. Romanenko ²⁵, F. Ronchetti ³², D. Rosales Herrera ⁴³, E.D. Rosas ⁶⁴, K. Roslon ¹³³, A. Rossi ⁵³,
A. Roy ⁴⁷, A. Roy ¹¹⁸, S. Roy ⁴⁶, N. Rubini ⁵⁰, O. Rubza ^{I,15}, J.A. Rudolph ⁸¹, D. Ruggiano ¹³³,
R. Rui ²³, P.G. Russek ², A. Rustamov ⁷⁸, A. Rybicki ¹⁰³, L.C.V. Ryder ¹¹⁴, G. Ryu ⁶⁹, J. Ryu ¹⁶,
W. Rzesza ⁹², B. Sabiu ⁵⁰, R. Sadek ⁷¹, S. Sadhu ⁴¹, A. Saha ³¹, S. Saha ⁷⁷, B. Sahoo ⁴⁷,
R. Sahoo ⁴⁷, D. Sahu ⁶⁴, P.K. Sahu ⁶⁰, J. Saini ¹³², S. Sakai ¹²², S. Sambyal ⁸⁸, D. Samitz ⁷³,
I. Sanna ³², D. Sarkar ⁸⁰, V. Sarritzu ²², V.M. Sarti ⁹², M.H.P. Sas ⁸¹, U. Savino ²⁴, S. Sawan ⁷⁷,
E. Scapparone ⁵⁰, J. Schambach ⁸⁴, H.S. Scheid ³², C. Schiaua ⁴⁴, R. Schicker ⁹¹, F. Schlepfer ^{32,91},
A. Schmah ⁹⁴, C. Schmidt ⁹⁴, M. Schmidt ⁹⁰, J. Schoengarth ⁶³, R. Schotter ⁷³, A. Schröter ³⁸,
J. Schukraft ³², K. Schweda ⁹⁴, G. Scioli ²⁵, E. Scomparin ⁵⁵, J.E. Seger ¹⁴, D. Sekihata ¹²¹,
M. Selina ⁸¹, I. Selyuzhenkov ⁹⁴, S. Senyukov ¹²⁶, J.J. Seo ⁹¹, L. Serkin ^{IX,64}, L. Šerkšnytė ³²,
A. Sevcenco ⁶², T.J. Shaba ⁶⁷, A. Shabetai ⁹⁹, R. Shahoyan ³², B. Sharma ⁸⁸, D. Sharma ⁴⁶,
H. Sharma ⁵³, M. Sharma ⁸⁸, S. Sharma ⁸⁸, T. Sharma ⁴⁰, U. Sharma ⁸⁸, O. Sheibani ¹³⁴, K. Shigaki ⁸⁹,
M. Shimomura ⁷⁵, Q. Shou ³⁹, S. Siddhanta ⁵¹, T. Siemiarz ⁷⁶, T.F. Silva ¹⁰⁶, W.D. Silva ¹⁰⁶,
D. Silvermyr ⁷², T. Simantathammakul ¹⁰¹, R. Simeonov ³⁵, B. Singh ⁴⁶, B. Singh ⁸⁸, B. Singh ⁹²,
K. Singh ⁴⁷, R. Singh ⁷⁷, R. Singh ⁵³, S. Singh ¹⁵, T. Sinha ⁹⁶, B. Sitar ¹³, M. Sitta ^{130,55},
T.B. Skaali ¹⁹, G. Skorodumovs ⁹¹, N. Smirnov ¹³⁵, K.L. Smith ¹⁶, R.J.M. Snellings ⁵⁸,
E.H. Solheim ¹⁹, S. Solokhin ⁸¹, C. Sonnabend ^{32,94}, J.M. Sonneveld ⁸¹, F. Soramel ²⁷,
A.B. Soto-Hernandez ⁸⁵, R. Spijkers ⁸¹, C. Sporleder ¹¹³, I. Sputowska ¹⁰³, J. Staa ⁷², J. Stachel ⁹¹,
L.L. Stahl ¹⁰⁶, I. Stan ⁶², A.G. Stejskal ¹¹⁴, T. Stellhorn ¹²³, S.F. Stiefelmaier ⁹¹, D. Stocco ⁹⁹,
I. Storehaug ¹⁹, N.J. Strangmann ⁶³, P. Stratmann ¹²³, S. Strazzi ²⁵, A. Sturniolo ^{115,30,52}, Y. Su ⁶,
A.A.P. Suaide ¹⁰⁶, C. Suire ¹²⁸, A. Suiu ¹⁰⁹, M. Sukhanov ¹³⁹, M. Suljic ³², V. Sumberia ⁸⁸,
S. Sumowidagdo ⁷⁹, P. Sun ¹⁰, N.B. Sundstrom ⁵⁸, L.H. Tabares ⁷, A. Tabikh ⁷⁰, S.F. Taghavi ⁹²,
J. Takahashi ¹⁰⁷, M.A. Talamantes Johnson ⁴³, G.J. Tambave ⁷⁷, Z. Tang ¹¹⁶, J. Tanwar ⁸⁷, J.D. Tapia
Takaki ¹¹⁴, N. Tapus ¹⁰⁹, L.A. Tarasovicova ³⁶, M.G. Tarzila ⁴⁴, A. Tauro ³², A. Távira García ^{104,128},
G. Tejeda Muñoz ⁴³, L. Terlizzi ²⁴, C. Terrevoli ⁴⁹, D. Thakur ⁵⁵, S. Thakur ⁴, M. Thogersen ¹⁹,
D. Thomas ¹⁰⁴, A.M. Tiekoetter ¹²³, N. Tiltmann ^{32,123}, A.R. Timmins ¹¹², A. Toia ⁶³, R. Tokumoto ⁸⁹,
S. Tomassini ²⁵, K. Tomohiro ⁸⁹, Q. Tong ⁶, V.V. Torres ⁹⁹, A. Trifiró ^{30,52}, T. Triloki ⁹³, A.S. Triolo ³²,
S. Tripathy ³², T. Tripathy ¹²⁴, S. Trogolo ²⁴, V. Trubnikov ³, W.H. Trzaska ¹¹³, T.P. Trzcinski ¹³³,
C. Tzolanta ¹⁹, R. Tu ³⁹, R. Turrisi ⁵³, T.S. Tveter ¹⁹, K. Ullaland ²⁰, B. Ulukutlu ⁹², S. Upadhyaya ¹⁰³,
A. Uras ¹²⁵, M. Urioni ²³, G.L. Usai ²², M. Vaid ⁸⁸, M. Vala ³⁶, N. Valle ⁵⁴, L.V.R. van Doremalen ⁵⁸,
M. van Leeuwen ⁸¹, C.A. van Veen ⁹¹, R.J.G. van Weelden ⁸¹, D. Varga ⁴⁵, Z. Varga ¹³⁵,
P. Vargas Torres ⁶⁴, O. Vázquez Doce ⁴⁸, O. Vazquez Rueda ¹¹², G. Vecil ²³, P. Veen ¹²⁷,
E. Vercellin ²⁴, R. Verma ⁴⁶, R. Vértesi ⁴⁵, M. Verweij ⁵⁸, L. Vickovic ³³, Z. Vilakazi ¹²⁰, A. Villani ²³,
C.J.D. Villiers ⁶⁷, T. Virgili ²⁸, M.M.O. Virta ⁴², A. Vodopyanov ¹³⁹, M.A. Völkl ⁹⁷, S.A. Voloshin ¹³⁴,
G. Volpe ³¹, B. von Haller ³², I. Vorobyev ³², N. Vozniuk ¹³⁹, J. Vrláková ³⁶, J. Wan ³⁹, C. Wang ³⁹,
D. Wang ³⁹, Y. Wang ¹¹⁶, Y. Wang ³⁹, Y. Wang ⁶, Z. Wang ³⁹, F. Weiglhofer ³², S.C. Wenzel ³²,
J.P. Wessels ¹²³, P.K. Wiacek ², J. Wiechula ⁶³, J. Wikne ¹⁹, G. Wilk ⁷⁶, J. Wilkinson ⁹⁴,
G.A. Willems ¹²³, N. Wilson ¹¹⁵, B. Windelband ⁹¹, J. Witte ⁹¹, M. Wojnar ², C.I. Worek ²,
J.R. Wright ¹⁰⁴, C.-T. Wu ^{6,27}, W. Wu ^{92,39}, Y. Wu ¹¹⁶, K. Xiong ³⁹, Z. Xiong ¹¹⁶, L. Xu ^{125,6}, R. Xu ⁶,
Z. Xue ⁷¹, A. Yadav ⁴¹, A.K. Yadav ¹³², Y. Yamaguchi ⁸⁹, S. Yang ⁵⁷, S. Yang ²⁰, S. Yano ⁸⁹,
Z. Ye ⁷¹, E.R. Yeats ¹⁸, J. Yi ⁶, R. Yin ³⁹, Z. Yin ⁶, I.-K. Yoo ¹⁶, J.H. Yoon ⁵⁷, H. Yu ¹², S. Yuan ²⁰,
A. Yuncu ⁹¹, V. Zaccolo ²³, C. Zampolli ³², F. Zanone ⁹¹, N. Zardoshti ³², P. Závada ⁶¹, B. Zhang ⁹¹,
C. Zhang ¹²⁷, M. Zhang ^{124,6}, M. Zhang ^{27,6}, S. Zhang ³⁹, X. Zhang ⁶, Y. Zhang ¹¹⁶, Y. Zhang ¹¹⁶,
Z. Zhang ⁶, D. Zhou ⁶, Y. Zhou ⁸⁰, Z. Zhou ³⁹, J. Zhu ³⁹, S. Zhu ^{94,116}, Y. Zhu ⁶, A. Zingaretti ²⁷,
S.C. Zugravel ⁵⁵, N. Zurlo ^{131,54}

Affiliation Notes

- ^I Deceased
- ^{II} Also at: INFN Trieste
- ^{III} Also at: Max-Planck-Institut für Physik, Munich, Germany
- ^{IV} Also at: Czech Technical University in Prague (CZ)
- ^V Also at: Instituto de Física da Universidade de São Paulo
- ^{VI} Also at: Dipartimento DET del Politecnico di Torino, Turin, Italy
- ^{VII} Also at: Department of Applied Physics, Aligarh Muslim University, Aligarh, India
- ^{VIII} Also at: Institute of Theoretical Physics, University of Wrocław, Poland
- ^{IX} Also at: Facultad de Ciencias, Universidad Nacional Autónoma de México, Mexico City, Mexico

Collaboration Institutes

- ¹ A.I. Alikhanyan National Science Laboratory (Yerevan Physics Institute) Foundation, Yerevan, Armenia
- ² AGH University of Krakow, Cracow, Poland
- ³ Bogolyubov Institute for Theoretical Physics, National Academy of Sciences of Ukraine, Kyiv, Ukraine
- ⁴ Bose Institute, Department of Physics and Centre for Astroparticle Physics and Space Science (CAPSS), Kolkata, India
- ⁵ California Polytechnic State University, San Luis Obispo, California, United States
- ⁶ Central China Normal University, Wuhan, China
- ⁷ Centro de Aplicaciones Tecnológicas y Desarrollo Nuclear (CEADEN), Havana, Cuba
- ⁸ Centro de Investigación y de Estudios Avanzados (CINVESTAV), Mexico City and Mérida, Mexico
- ⁹ Chicago State University, Chicago, Illinois, United States
- ¹⁰ China Nuclear Data Center, China Institute of Atomic Energy, Beijing, China
- ¹¹ China University of Geosciences, Wuhan, China
- ¹² Chungbuk National University, Cheongju, Republic of Korea
- ¹³ Comenius University Bratislava, Faculty of Mathematics, Physics and Informatics, Bratislava, Slovak Republic
- ¹⁴ Creighton University, Omaha, Nebraska, United States
- ¹⁵ Department of Physics, Aligarh Muslim University, Aligarh, India
- ¹⁶ Department of Physics, Pusan National University, Pusan, Republic of Korea
- ¹⁷ Department of Physics, Sejong University, Seoul, Republic of Korea
- ¹⁸ Department of Physics, University of California, Berkeley, California, United States
- ¹⁹ Department of Physics, University of Oslo, Oslo, Norway
- ²⁰ Department of Physics and Technology, University of Bergen, Bergen, Norway
- ²¹ Dipartimento di Fisica, Università di Pavia, Pavia, Italy
- ²² Dipartimento di Fisica dell'Università and Sezione INFN, Cagliari, Italy
- ²³ Dipartimento di Fisica dell'Università and Sezione INFN, Trieste, Italy
- ²⁴ Dipartimento di Fisica dell'Università and Sezione INFN, Turin, Italy
- ²⁵ Dipartimento di Fisica e Astronomia dell'Università and Sezione INFN, Bologna, Italy
- ²⁶ Dipartimento di Fisica e Astronomia dell'Università and Sezione INFN, Catania, Italy
- ²⁷ Dipartimento di Fisica e Astronomia dell'Università and Sezione INFN, Padova, Italy
- ²⁸ Dipartimento di Fisica 'E.R. Caianiello' dell'Università and Gruppo Collegato INFN, Salerno, Italy
- ²⁹ Dipartimento DISAT del Politecnico and Sezione INFN, Turin, Italy
- ³⁰ Dipartimento di Scienze MIFT, Università di Messina, Messina, Italy
- ³¹ Dipartimento Interateneo di Fisica 'M. Merlin' and Sezione INFN, Bari, Italy
- ³² European Organization for Nuclear Research (CERN), Geneva, Switzerland
- ³³ Faculty of Electrical Engineering, Mechanical Engineering and Naval Architecture, University of Split, Split, Croatia
- ³⁴ Faculty of Nuclear Sciences and Physical Engineering, Czech Technical University in Prague, Prague, Czech Republic
- ³⁵ Faculty of Physics, Sofia University, Sofia, Bulgaria
- ³⁶ Faculty of Science, P.J. Šafárik University, Košice, Slovak Republic
- ³⁷ Faculty of Technology, Environmental and Social Sciences, Bergen, Norway
- ³⁸ Frankfurt Institute for Advanced Studies, Johann Wolfgang Goethe-Universität Frankfurt, Frankfurt, Germany
- ³⁹ Fudan University, Shanghai, China
- ⁴⁰ Gauhati University, Department of Physics, Guwahati, India

- 41 Helmholtz-Institut für Strahlen- und Kernphysik, Rheinische Friedrich-Wilhelms-Universität Bonn, Bonn, Germany
- 42 Helsinki Institute of Physics (HIP), Helsinki, Finland
- 43 High Energy Physics Group, Universidad Autónoma de Puebla, Puebla, Mexico
- 44 Horia Hulubei National Institute of Physics and Nuclear Engineering, Bucharest, Romania
- 45 HUN-REN Wigner Research Centre for Physics, Budapest, Hungary
- 46 Indian Institute of Technology Bombay (IIT), Mumbai, India
- 47 Indian Institute of Technology Indore, Indore, India
- 48 INFN, Laboratori Nazionali di Frascati, Frascati, Italy
- 49 INFN, Sezione di Bari, Bari, Italy
- 50 INFN, Sezione di Bologna, Bologna, Italy
- 51 INFN, Sezione di Cagliari, Cagliari, Italy
- 52 INFN, Sezione di Catania, Catania, Italy
- 53 INFN, Sezione di Padova, Padova, Italy
- 54 INFN, Sezione di Pavia, Pavia, Italy
- 55 INFN, Sezione di Torino, Turin, Italy
- 56 INFN, Sezione di Trieste, Trieste, Italy
- 57 Inha University, Incheon, Republic of Korea
- 58 Institute for Gravitational and Subatomic Physics (GRASP), Utrecht University/Nikhef, Utrecht, Netherlands
- 59 Institute of Experimental Physics, Slovak Academy of Sciences, Košice, Slovak Republic
- 60 Institute of Physics, Homi Bhabha National Institute, Bhubaneswar, India
- 61 Institute of Physics of the Czech Academy of Sciences, Prague, Czech Republic
- 62 Institute of Space Science (ISS), Bucharest, Romania
- 63 Institut für Kernphysik, Johann Wolfgang Goethe-Universität Frankfurt, Frankfurt, Germany
- 64 Instituto de Ciencias Nucleares, Universidad Nacional Autónoma de México, Mexico City, Mexico
- 65 Instituto de Física, Universidade Federal do Rio Grande do Sul (UFRGS), Porto Alegre, Brazil
- 66 Instituto de Física, Universidad Nacional Autónoma de México, Mexico City, Mexico
- 67 iThemba LABS, National Research Foundation, Somerset West, South Africa
- 68 Jeonbuk National University, Jeonju, Republic of Korea
- 69 Korea Institute of Science and Technology Information, Daejeon, Republic of Korea
- 70 Laboratoire de Physique Subatomique et de Cosmologie, Université Grenoble-Alpes, CNRS-IN2P3, Grenoble, France
- 71 Lawrence Berkeley National Laboratory, Berkeley, California, United States
- 72 Lund University Department of Physics, Division of Particle Physics, Lund, Sweden
- 73 Marietta Blau Institute, Vienna, Austria
- 74 Nagasaki Institute of Applied Science, Nagasaki, Japan
- 75 Nara Women's University (NWU), Nara, Japan
- 76 National Centre for Nuclear Research, Warsaw, Poland
- 77 National Institute of Science Education and Research, Homi Bhabha National Institute, Jatni, India
- 78 National Nuclear Research Center, Baku, Azerbaijan
- 79 National Research and Innovation Agency - BRIN, Jakarta, Indonesia
- 80 Niels Bohr Institute, University of Copenhagen, Copenhagen, Denmark
- 81 Nikhef, National institute for subatomic physics, Amsterdam, Netherlands
- 82 Nuclear Physics Group, STFC Daresbury Laboratory, Daresbury, United Kingdom
- 83 Nuclear Physics Institute of the Czech Academy of Sciences, Husinec-Řež, Czech Republic
- 84 Oak Ridge National Laboratory, Oak Ridge, Tennessee, United States
- 85 Ohio State University, Columbus, Ohio, United States
- 86 Physics department, Faculty of science, University of Zagreb, Zagreb, Croatia
- 87 Physics Department, Panjab University, Chandigarh, India
- 88 Physics Department, University of Jammu, Jammu, India
- 89 Physics Program and International Institute for Sustainability with Knotted Chiral Meta Matter (WPI-SKCM²), Hiroshima University, Hiroshima, Japan
- 90 Physikalisches Institut, Eberhard-Karls-Universität Tübingen, Tübingen, Germany
- 91 Physikalisches Institut, Ruprecht-Karls-Universität Heidelberg, Heidelberg, Germany
- 92 Physik Department, Technische Universität München, Munich, Germany
- 93 Politecnico di Bari and Sezione INFN, Bari, Italy

- ⁹⁴ Research Division and ExtreMe Matter Institute EMMI, GSI Helmholtzzentrum für Schwerionenforschung GmbH, Darmstadt, Germany
- ⁹⁵ Saga University, Saga, Japan
- ⁹⁶ Saha Institute of Nuclear Physics, Homi Bhabha National Institute, Kolkata, India
- ⁹⁷ School of Physics and Astronomy, University of Birmingham, Birmingham, United Kingdom
- ⁹⁸ Sección Física, Departamento de Ciencias, Pontificia Universidad Católica del Perú, Lima, Peru
- ⁹⁹ SUBATECH, IMT Atlantique, Nantes Université, CNRS-IN2P3, Nantes, France
- ¹⁰⁰ Sungkyunkwan University, Suwon City, Republic of Korea
- ¹⁰¹ Suranaree University of Technology, Nakhon Ratchasima, Thailand
- ¹⁰² Technical University of Košice, Košice, Slovak Republic
- ¹⁰³ The Henryk Niewodniczanski Institute of Nuclear Physics, Polish Academy of Sciences, Cracow, Poland
- ¹⁰⁴ The University of Texas at Austin, Austin, Texas, United States
- ¹⁰⁵ Universidad Autónoma de Sinaloa, Culiacán, Mexico
- ¹⁰⁶ Universidade de São Paulo (USP), São Paulo, Brazil
- ¹⁰⁷ Universidade Estadual de Campinas (UNICAMP), Campinas, Brazil
- ¹⁰⁸ Universidade Federal do ABC, Santo Andre, Brazil
- ¹⁰⁹ Universitatea Nationala de Stiinta si Tehnologie Politehnica Bucuresti, Bucharest, Romania
- ¹¹⁰ University of Cape Town, Cape Town, South Africa
- ¹¹¹ University of Derby, Derby, United Kingdom
- ¹¹² University of Houston, Houston, Texas, United States
- ¹¹³ University of Jyväskylä, Jyväskylä, Finland
- ¹¹⁴ University of Kansas, Lawrence, Kansas, United States
- ¹¹⁵ University of Liverpool, Liverpool, United Kingdom
- ¹¹⁶ University of Science and Technology of China, Hefei, China
- ¹¹⁷ University of Silesia in Katowice, Katowice, Poland
- ¹¹⁸ University of South-Eastern Norway, Kongsberg, Norway
- ¹¹⁹ University of Tennessee, Knoxville, Tennessee, United States
- ¹²⁰ University of the Witwatersrand, Johannesburg, South Africa
- ¹²¹ University of Tokyo, Tokyo, Japan
- ¹²² University of Tsukuba, Tsukuba, Japan
- ¹²³ Universität Münster, Institut für Kernphysik, Münster, Germany
- ¹²⁴ Université Clermont Auvergne, CNRS/IN2P3, LPC, Clermont-Ferrand, France
- ¹²⁵ Université de Lyon, CNRS/IN2P3, Institut de Physique des 2 Infinis de Lyon, Lyon, France
- ¹²⁶ Université de Strasbourg, CNRS, IPHC UMR 7178, F-67000 Strasbourg, France, Strasbourg, France
- ¹²⁷ Université Paris-Saclay, Centre d'Etudes de Saclay (CEA), IRFU, Département de Physique Nucléaire (DPhN), Saclay, France
- ¹²⁸ Université Paris-Saclay, CNRS/IN2P3, IJCLab, Orsay, France
- ¹²⁹ Università degli Studi di Foggia, Foggia, Italy
- ¹³⁰ Università del Piemonte Orientale, Vercelli, Italy
- ¹³¹ Università di Brescia, Brescia, Italy
- ¹³² Variable Energy Cyclotron Centre, Homi Bhabha National Institute, Kolkata, India
- ¹³³ Warsaw University of Technology, Warsaw, Poland
- ¹³⁴ Wayne State University, Detroit, Michigan, United States
- ¹³⁵ Yale University, New Haven, Connecticut, United States
- ¹³⁶ Yildiz Technical University, Istanbul, Turkey
- ¹³⁷ Yonsei University, Seoul, Republic of Korea
- ¹³⁸ Affiliated with an institute formerly covered by a cooperation agreement with CERN
- ¹³⁹ Affiliated with an international laboratory covered by a cooperation agreement with CERN.